Velocity Analysis of Multi-Receiver Full Waveform Acoustic Logging Data In Open and Cased Holes

by

Lisa V. Block, C.H. Cheng, and Gregory L. Duckworth

Earth Resources Laboratory
Department of Earth, Atmospheric, and Planetary Sciences
Massachusetts Institute of Technology
Cambridge, MA 02139

ABSTRACT

Average semblance and maximum-likelihood spectral analyses are applied to synthetic and field full waveform acoustic logging data to determine formation velocities. Of particular interest is the ability of these methods to resolve the P and shear/pseudo-Rayleigh arrivals in data from poorly-bonded cased boreholes. In synthetic open-hole data the velocity analyses yield results within 4% of the true velocities. Results from synthetic well-bonded cased hole data are generally as good as those from the open hole data. However, if the formation P-wave velocity is within roughly 10% of the plate velocity of the steel pipe (about 5.3—5.5 km/s), then there may be a resonance effect that appears to slow down the P wave slightly (on the order of 6%). For cased-hole models with no steel/cement bonding (the free-pipe situation), the measured P-wave velocities are typically 6 to 8% less than the actual formation velocities. If the formation S-wave velocity is greater than about 2.5 km/s, the S-wave velocity estimate may also be 6 to 8% low. Furthermore, increasing the thickness of either the cement layer or the fluid layer between the pipe and the cement further decreases the formation velocity estimates. Also, if the P-wave velocity is within roughly 15% of the velocity of the steel arrival, the P wave may not be resolved by the semblance method unless the data is first low-pass filtered. Initial tests show that this filtering process may adversely affect the final P-wave velocity estimate, but the details of this type of approach have not been studied. The P wave is resolved by spectral analysis of the original, unfiltered data. For cased-hole models with no cement/formation bonding (the unbonded-casing

situation), formation S-wave velocities are estimated to within 3% relative error, and the formation P-wave velocity is estimated to within 2% error in a slow formation. However, for P-wave velocities between 3.4 km/s and 5.94 km/s, the P wave cannot be resolved by spectral analysis, and it is resolved by the semblance method only in the model with the low velocity (3.4 km/s).

INTRODUCTION

This paper is a continuation of the work begun last year in velocity analysis of full waveform acoustic logging data. Two methods of velocity analysis are employed: the maximum-likelihood method (MLM), which is a high-resolution spectral method, and the average semblance method. A description of these methods is given in the Appendix. Additional information on the maximum-likelihood method can be found in Duckworth (1983). The objective of this work is two-fold: to determine borehole conditions which allow estimation of formation velocities from full waveform acoustic well logs, and to compare the performances of the maximum-likelihood method and the semblance method. Synthetic data sets for open-hole models, well-bonded cased-hole models, and poorly-bonded cased-hole models are generated using the method of Tubman (1984). (The frequency range of the source function is approximately 4 to 18 kHz.) For each case, models with varying formation velocities are studied. Both velocity analysis techniques are applied to each data set and the results are compared. In this report, the results for the open-hole models and the well-bonded cased-hole models are briefly summarized. The results for the poorly-bonded cased-hole models are presented in more detail. These models are divided into two groups: those models in which the steel pipe is not bonded to the cement, referred to as the free-pipe situation, and those models in which the cement is not bonded to the formation, referred to as the unbonded-casing situation. Finally, field data from open and cased holes are analyzed.

RESULTS

Open-hole and Well-bonded Cased-hole Models

Data from open-borehole models have been analyzed for formation P-wave velocities of 4.0 km/s, 4.88 km/s, and 5.94 km/s. (The corresponding S-wave velocities are 2.13 km/s, 2.6 km/s, and 3.2 km/s.) The P wave and the shear/pseudo-Rayleigh wave are resolved well by both methods. The formation velocities are determined to within 4% of the true velocities. The Stoneley wave is resolved by the maximum-likelihood method at the lowest frequency analyzed, 4 kHz. It is not resolved by the MLM results at higher

frequencies, or in the semblance plot. Data from well-bonded cased-hole models with exactly the same formation parameters as the open-hole models were analyzed. The results computed from well-bonded cased-hole data are very similar to those calculated from the open-hole data. The main difference is that in the results from the cased-hole data, the Stoneley wave is resolved in the semblance plot and in the MLM plots at frequencies up to 16 kHz. This is largely because the presence of the casing decreases the effective radius of the borehole, resulting in an apparent shift of the dispersion behavior to higher frequencies (Cheng and Toksöz, 1981). Thus, the pseudo-Rayleigh wave is excited to a lesser extent, and the Stoneley wave to a larger extent, over the frequency range of the source function in cased-hole models than in open-hole models. Also, the rigid steel pipe may act as a more efficient waveguide for the Stoneley wave than the fluid/formation boundary in the open borehole. In general, the formation velocities determined from the well-bonded cased-hole data differ only slightly from those found from the open-hole data. However, a rather significant deviation occurs for the model with the high formation velocities (P-wave velocity = 5.94 km/s, S-wave velocity = 3.2 km/s). The microseismograms for this model exhibit a moderate amount of ringing, resulting from the fact that the formation P-wave velocity is close to the velocity of the steel pipe. Tubman (1984) shows that the character of the ringing depends upon the source function used. In this case the velocity spectra calculated from the cased-hole data yield a P-wave velocity of about 5.6 km/s, 6% less than the formation velocity, and the maximum on the semblance curve corresponding to the P wave lies between about 5.5 km/s and 5.8 km/s. In contrast, the results from analysis of the corresponding open-hole data give a much more accurate formation P-wave velocity estimate of about 5.85 to 5.9 km/s (by both methods).

Free-pipe Models

Data for the same three formations were analyzed for the free-pipe situation. The free-pipe situation is modelled by including a fluid layer between the steel pipe and the cement casing. Figure 1 shows the microseismograms for the first formation: the P-wave velocity is 4.00 km/s, and the S-wave velocity is 2.13 km/s. Also shown in Figure 1 are the radii, velocities, densities, and attenuation factors of the fluid, steel, and cement layers used in the model. The first arrival is that of a disturbance traveling through the steel. This arrival completely obscures the P wave. The pseudo-Rayleigh arrival is clear. Figure 2a contains the velocity spectrum at 12 kHz. Four peaks can be clearly seen. The broad peak centered at 0.7 ms and having a velocity of about 5.1 km/s corresponds to the steel arrival. The peak at 1.1 ms with a velocity of 3.75 km/s represents the P wave. This velocity is 6% less than the formation P-wave velocity of 4.00 km/s, perhaps indicating some influence of the cement and fluid layers on the propagation of the P wave. (Recall that analysis of the corresponding open-hole data yields a P-wave velocity of 3.95 km/s. Also, analysis of the well-bonded cased-hole data

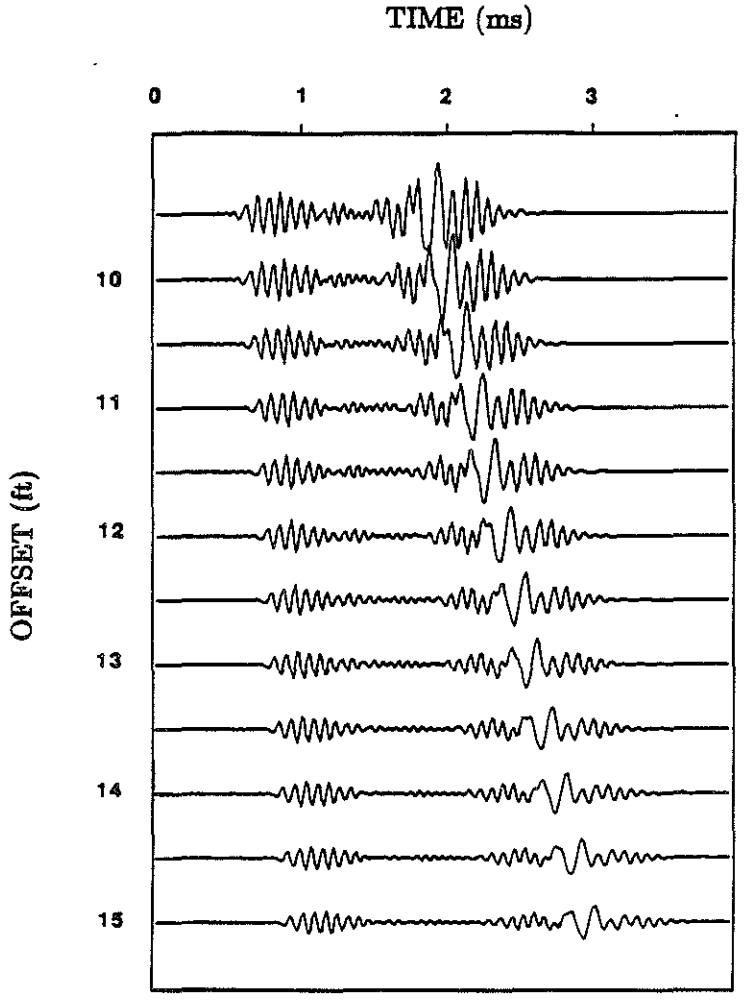

MODEL PARAMETERS

LAYER	OUTER RADIUS (cm)	V_p (km/s)	V_s (km/s)	DENSITY (g/cc)	Q_p	Q_s
fluid	4.699	1.68	0.00	1.20	20.00	0.00
steel	5.715	6.10	3.35	7.50	1000.00	1000.00
fluid	6.985	1.68	0.00	1.20	20.00	0.00
cement	10.160	2.82	1.73	1.92	40.00	30.00
formation	∞	4.00	2.13	2.16	60.00	60.00

sampling interval = 15.625 μs

Figure 1: Data for a free-pipe model.

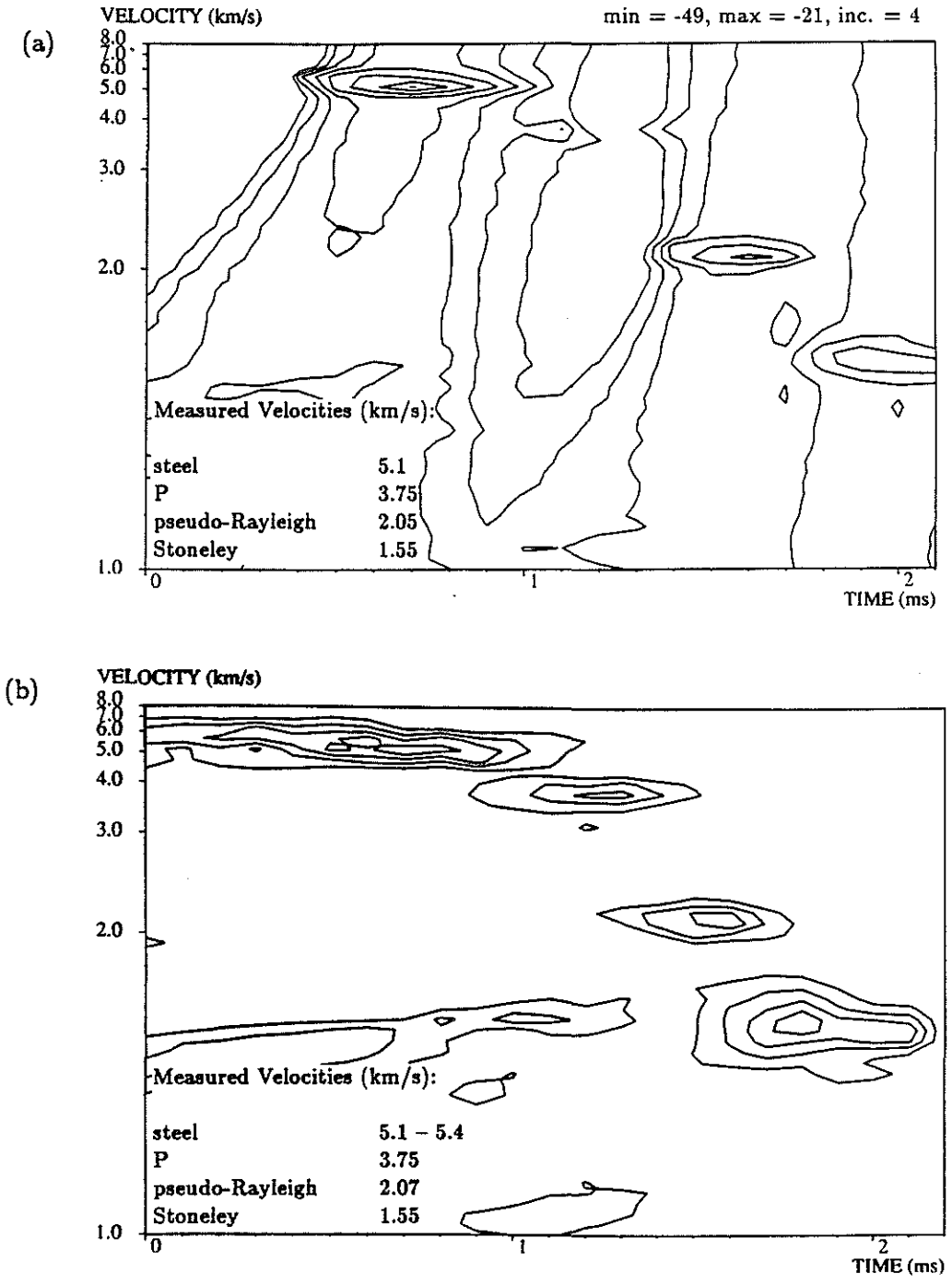

Figure 2: Velocity analysis of the data in Figure 1. (a) Velocity spectrum at 12 kHz. (b) Semblance.

yields a P-wave velocity of about 3.95 to 4.0 km/s.) The pseudo-Rayleigh wave comes in at about 1.6 ms with a velocity of 2.05 km/s, about 3.8% less than the true S-wave velocity of 2.13 km/s. (Velocity analysis of the corresponding well-bonded cased-hole data at this frequency yields a velocity estimate of approximately 2.14 km/s. Since the change in borehole radius due to the casing shifts the dispersion curve of the pseudo-Rayleigh wave, direct comparison to velocity estimates computed from the open-hole data cannot be made.) The Stoneley wave is represented by the large maximum at about 2 ms and 1.55 km/s. The semblance is presented in Figure 2b. The steel arrival, P wave, and Stoneley wave appear as strong peaks with the same velocities as in the velocity spectrum. (The Stoneley arrival is located at 1.8 ms. The linear feature to the left of the Stoneley wave is due to cycle-skipping across the steel arrival.) The peak representing the pseudo-Rayleigh arrival occurs at a velocity of 2.07 km/s.

A model having the same geometry as that just discussed but having higher formation velocities is examined. The P-wave velocity for this model is 4.88 km/s, and the S-wave velocity is 2.60 km/s. The data is presented in Figure 3. The duration of the steel arrival is greater than in the previous model, and therefore the pseudo-Rayleigh arrival is not as clear as before. The velocity spectra and semblance are shown in Figures 4a–d. The maximum in the extreme upper left corner of Figure 4a (velocity spectrum at 8 kHz) is due to slight noncausality in the synthetic data. The true steel arrival corresponds to the peak at 0.6 ms and 5.3 km/s. The P wave is represented by a small peak at 1.05 ms and 4.5 km/s. Again, the measured P-wave velocity is less than the formation velocity (by almost 8%). (Analysis of the corresponding open-hole data gives a P-wave velocity estimate of 4.7 to 4.8 km/s, and analysis of the well-bonded cased-hole data yields an estimate of 4.65 km/s.) The steel arrival and P-wave maxima begin to merge with increasing frequency. At 16 kHz (Figure 4c) the steel arrival is located at 0.8 ms and 5.1 km/s. The P-wave maximum has moved to 1.0 ms and approximately 4.65 km/s. The pseudo-Rayleigh wave is associated with a distinct peak at a velocity of about 2.45 km/s at all frequencies shown, 6% less than the formation S-wave velocity of 2.60 km/s. The semblance plot in Figure 4d yields the same S-wave velocity. (Velocity analysis of the corresponding well-bonded cased-hole data yields S-wave velocity estimates between 2.52 and 2.65 km/s.) No distinct P-wave maximum is present in the semblance results. The steel arrival and the P wave are represented by a linear feature varying in velocity from 4.3 km/s to 5.4 km/s. Apparently the P-wave formation velocity is close enough to the plate velocity of steel to cause minor resolution problems in the frequency domain and a total loss of resolution in the time domain. The Stoneley wave maxima occur at a velocity of 1.55 km/s, the same velocity as determined for the model with the slower formation velocities. This fact agrees with the observation made by Tubman et al. (1984) that the casing, rather than the formation velocities, is the major influence on the Stoneley wave velocity.

Since the P wave is best resolved for the model above in the velocity spectra at the lower frequencies, an attempt was made to low-pass filter the data and process the

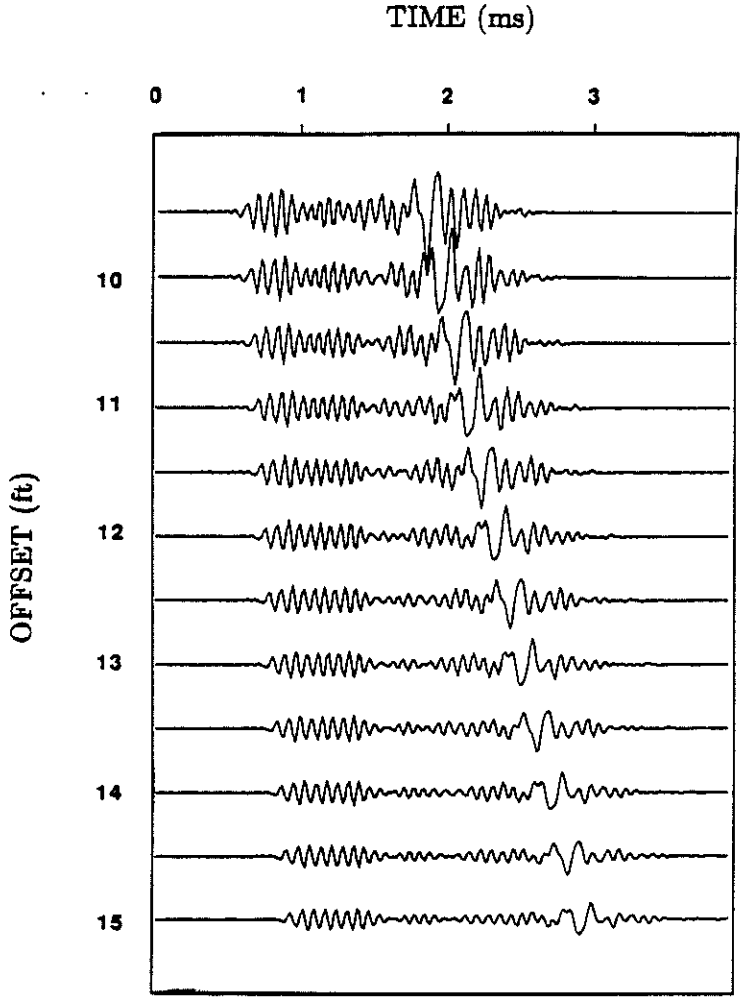

MODEL PARAMETERS

LAYER	OUTER RADIUS (cm)	V_p (km/s)	V_s (km/s)	DENSITY (g/cc)	Q_p	Q_s
fluid	4.699	1.68	0.00	1.20	20.00	0.00
steel	5.715	6.10	3.35	7.50	1000.00	1000.00
fluid	6.985	1.68	0.00	1.20	20.00	0.00
cement	10.160	2.82	1.73	1.92	40.00	30.00
formation	∞	4.88	2.60	2.16	60.00	60.00

sampling interval = 15.625 μs

Figure 3: Data for a free-pipe model. The borehole geometry is the same as that in Figure 1 but the formation velocities are higher.

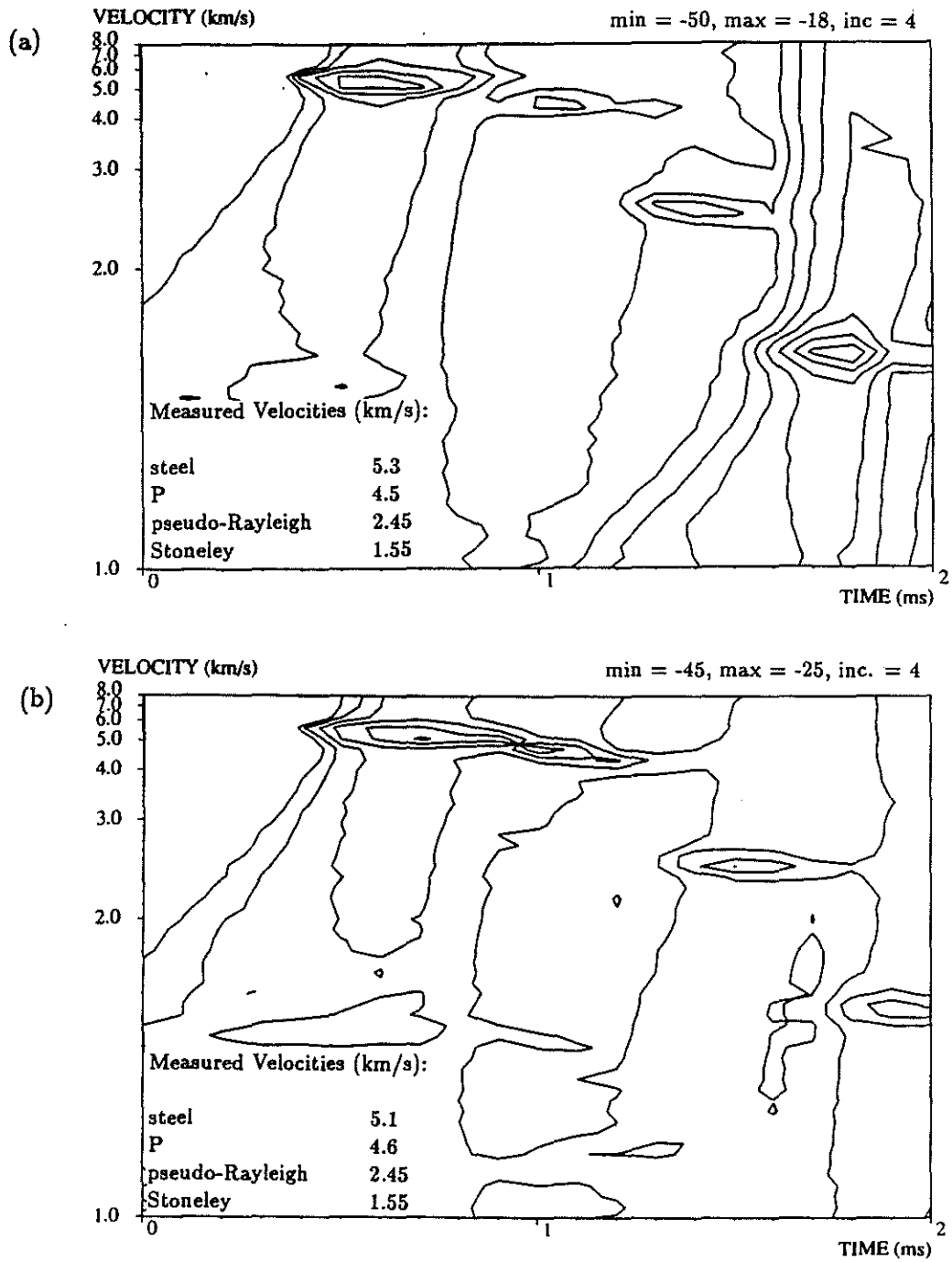

Figure 4: Velocity analysis of the data in Figure 3. (a) Velocity spectrum at 8 kHz. (b) Velocity spectrum at 12 kHz. (c) Velocity spectrum at 16 kHz. (d) Semblance.

(c)

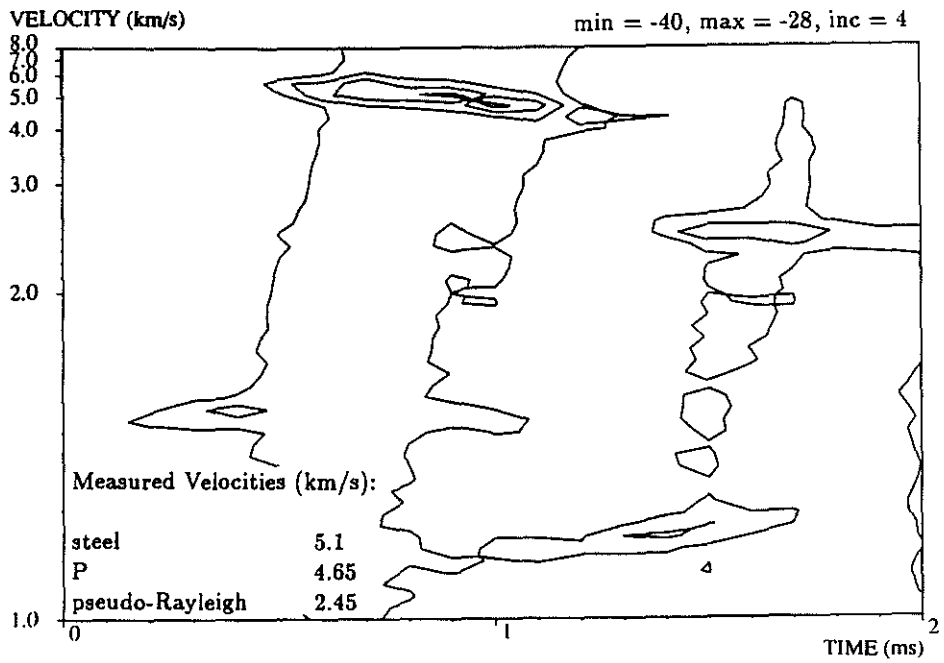
VELOCITY (km/s)
min = -40, max = -28, inc = 4
8.0
7.0
6.0
5.0
4.0
3.0
2.0
1.0
0
1
2
TIME (ms)
Measured Velocities (km/s):
steel 5.1
P 4.65
pseudo-Rayleigh 2.45

(d)

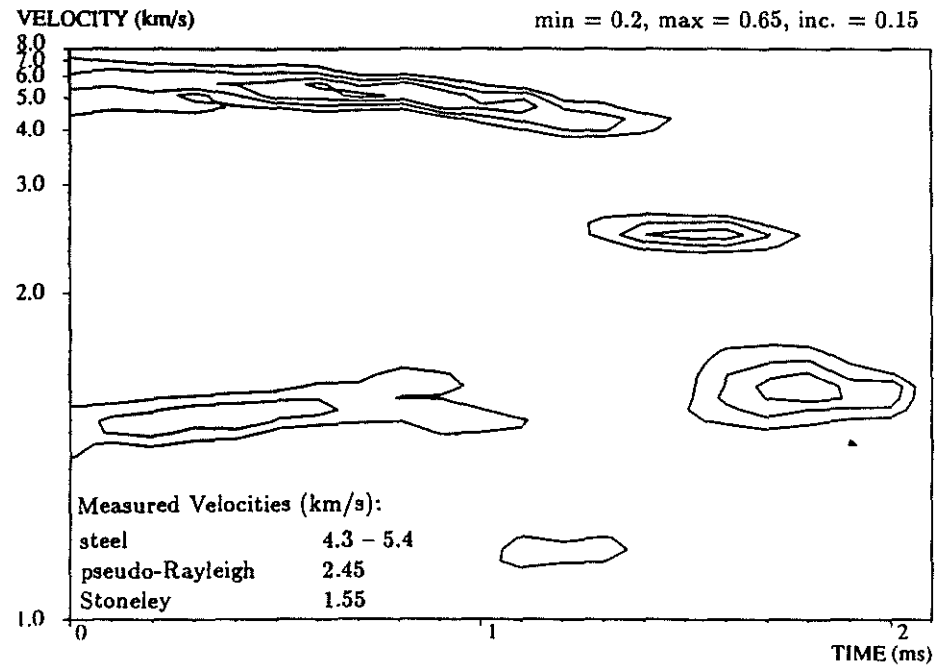
VELOCITY (km/s)
min = 0.2, max = 0.65, inc. = 0.15
8.0
7.0
6.0
5.0
4.0
3.0
2.0
1.0
0
1
2
TIME (ms)
Measured Velocities (km/s):
steel 4.3 – 5.4
pseudo-Rayleigh 2.45
Stoneley 1.55

filtered data to see if the P wave could then be resolved by the semblance method. The filter shown in Figure 5a was applied to the data to cut off the spectrum between 13 and 17 kHz. The filtered data is shown in Figure 5b. The ringing in the data has been reduced slightly. The results of the semblance are shown in Figure 5c. The P wave is now represented by a discernable peak at a velocity of about 4.6 km/s, as good as the velocity estimate obtained via MLM. If the data is filtered to a greater extent, such as shown in Figure 6, the P wave is better resolved in the semblance results. However, the P-wave velocity estimate is reduced. In Figure 6 the spectrum is cut off between 11 and 15 kHz, and the P-wave velocity estimate obtained from semblance is about 4.3 – 4.35 km/s. (The filtered data and the semblance results for this case are shown in Figures 6b and c.) In short, a P-wave velocity estimate may be obtained by filtering the data before applying semblance analysis, but the value of the estimate is sensitive to the filtering parameters.

For the model with the fast formation (P-wave velocity = 5.94 km/s; S-wave velocity = 3.2 km/s), a S-wave velocity estimate of about 2.95 km/s is obtained by both methods. This is 8% less the formation S-wave velocity. (Velocities between 3.1 and 3.2 km/s are measured in the open-hole situation.) No distinct P-wave maxima are present on the plots. Given the observation that the cement and fluid layers appear to slow down the P wave in the free-pipe situation, the P-wave energy is probably traveling with close to the velocity of the steel arrival, and hence the P wave is difficult to resolve with these methods.

In order to investigate the influence of the cement and fluid layers on the propagation of the P and shear/pseudo-Rayleigh waves, the thickness of the fluid layer was fixed at 1.27 cm while the thickness of the cement layer was varied from 3.175 cm to 4.4425 cm. Also, the thickness of the cement layer was fixed at 4.4425 cm while the thickness of the fluid layer was varied from 1.27 cm to 0.025 cm. This procedure was done for the first two formations above : P-wave velocity = 4.0 km/s (S-wave velocity = 2.13 km/s), and P-wave velocity = 4.88 km/s (S-wave velocity = 2.6 km/s). The results are summarized in Table 1. From these results it can be concluded that the estimated velocity of the P wave decreases as the thickness of either the fluid layer or the cement layer increases. Furthermore, the higher the P-wave velocity, the greater the absolute change in the velocity estimate as the geometry varies. Since the formation S-wave velocities are relatively low, changes in the velocity estimates of the shear or pseudo-Rayleigh waves with changes in the thicknesses of the fluid and cement layers are not significant in these examples. Indeed, the small changes that are observed may mainly be due to shifts in the dispersion curve of the pseudo-Rayleigh wave with changing effective borehole radius.

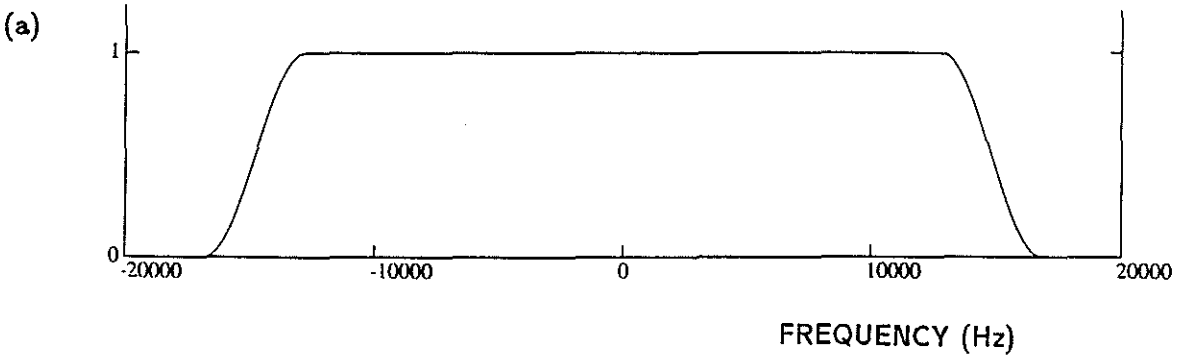

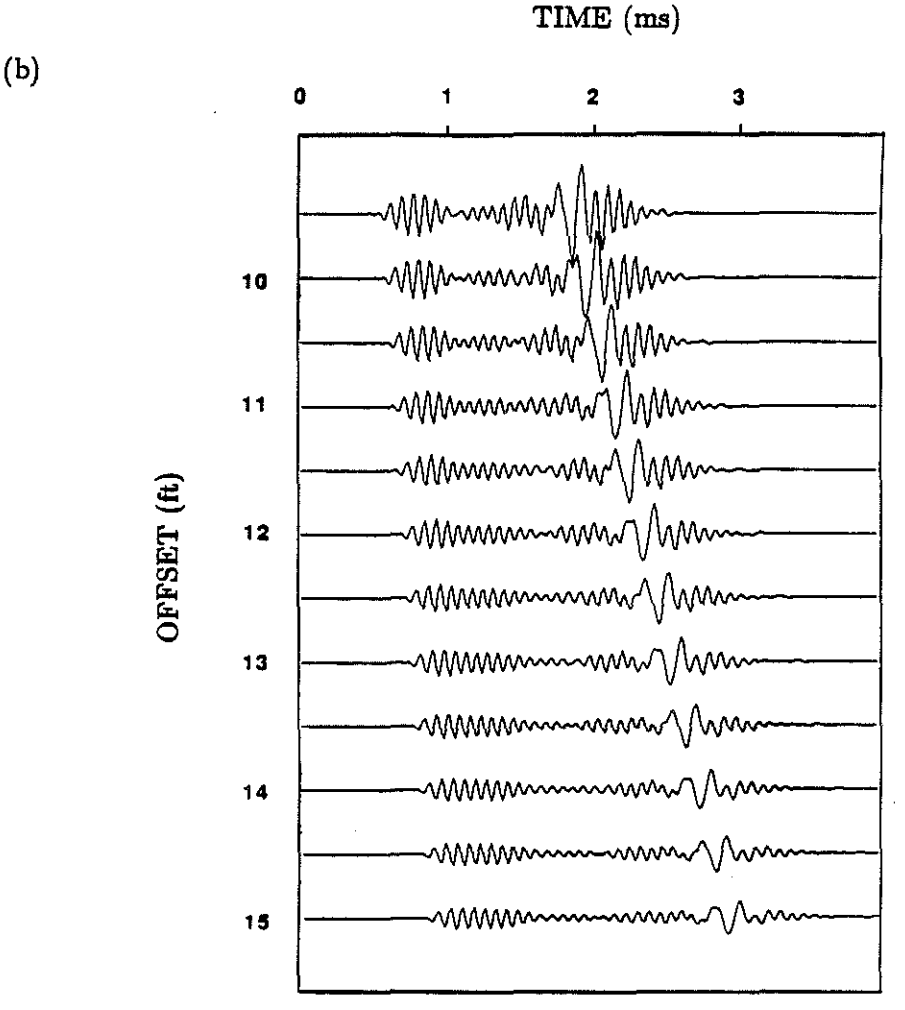

Figure 5: (a) Low-pass filter applied to the free-pipe data in Figure 3. (b) Filtered data. (c) Semblance results for the filtered data.

(c)

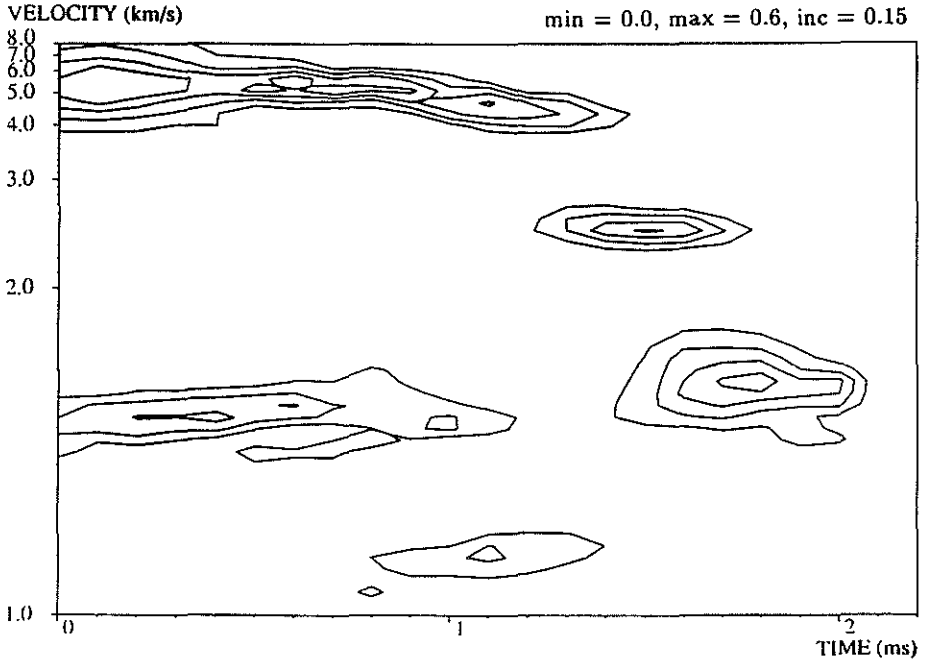
VELOCITY (km/s)
min = 0.0, max = 0.6, inc = 0.15
8.0
7.0
6.0
5.0
4.0
3.0
2.0
1.0
0
1
2
TIME (ms)

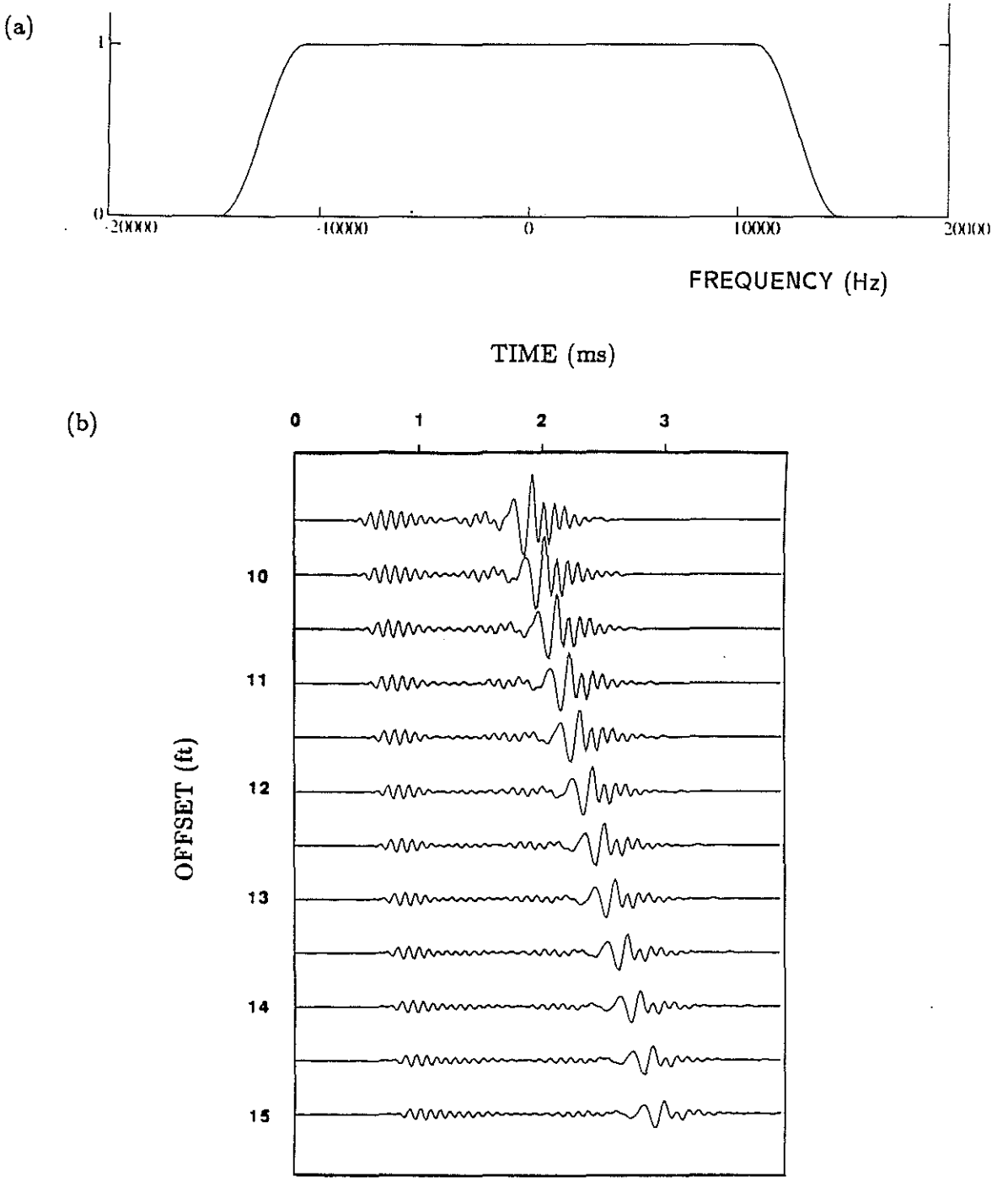

Figure 6: (a) Low-pass filter applied to the free-pipe data in Figure 3. (b) Filtered data. (c) Semblance results for the filtered data.

(c)

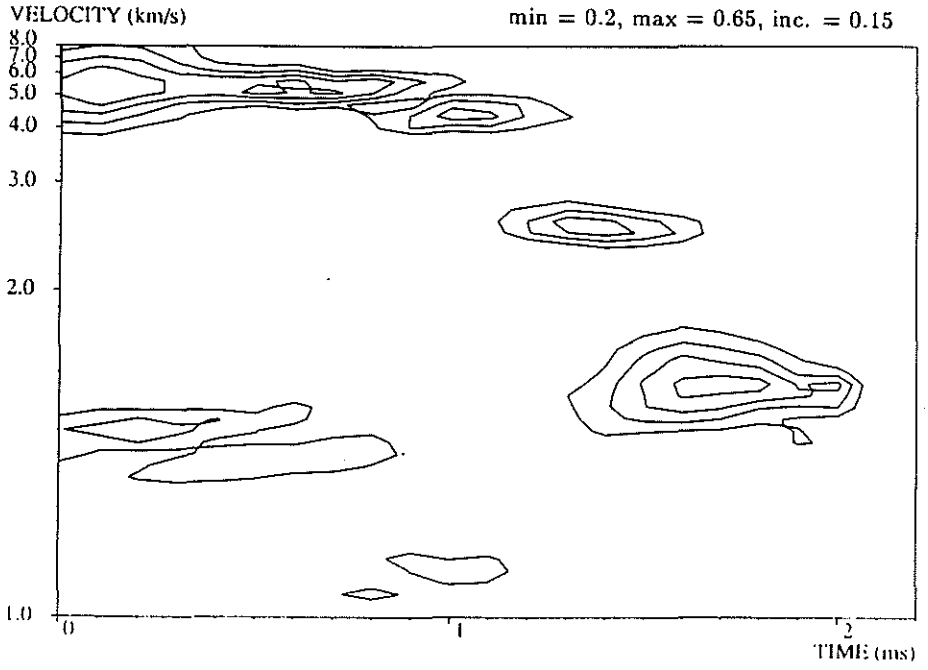
VELOCITY (km/s)
min = 0.2, max = 0.65, inc. = 0.15
8.0
7.0
6.0
5.0
4.0
3.0
2.0
1.0
0
1
2
TIME (ms)

Formation 1: *P-wave velocity = 4.00 km/s, S-wave velocity = 2.13 km/s*

Layer Thickness (cm)		Measured Velocity (km/s)	
cement	fluid	P	S
3.175	1.27	3.75	2.05 – 2.15
4.4425	1.27	3.5 – 3.6	2.03 – 2.09
4.4425	0.025	3.75	2.08 – 2.10

Formation 2: *P-wave velocity = 4.88 km/s, S-wave velocity = 2.60 km/s*

Layer Thickness (cm)		Measured Velocity (km/s)	
cement	fluid	P	S
3.175	1.27	4.5 – 4.65	2.45
4.4425	1.27	4.0 – 4.15	2.42 – 2.45
4.4425	0.025	4.3	2.45

Table 1: Comparison of the thicknesses of the fluid and cement layers in free-pipe situations and the velocity estimates obtained.

Models with Unbonded Casing

Good steel/cement bonding but no cement/formation bonding, referred to as the unbonded-casing situation, is modelled by inserting a fluid layer between the cement and the formation. Tubman (1984) showed that if the cement is sufficiently thick (on the order of 4 cm), it will damp out the casing arrival, and the P-wave arrival can be seen. However, if the cement is too thin, the first arrival on the microseismograms will be due to a disturbance propagating through the casing with a velocity intermediate between the steel and cement velocities. This situation can be observed in Figure 7. In this model, the thickness of the cement is 1.27 cm, and the thickness of the fluid layer is 3.18 cm. The complex nature of the first arrival is due to the combined ringing of the steel and the cement (Tubman, 1984). The amplitude variation within this arrival often causes its associated maxima on the velocity spectra to contain several subpeaks. The P-wave arrival is again completely obscured, and the pseudo-Rayleigh arrival is not clear. The formation P-wave velocity for this model is 4.00 km/s, and the S-wave velocity is 2.13 km/s. Figures 8a,b contain a typical velocity spectrum and the semblance plot. The maximum representing the pseudo-Rayleigh wave occurs at a velocity of about 2.08 km/s on the velocity spectrum and 2.15 km/s on the semblance plot. Hence, a

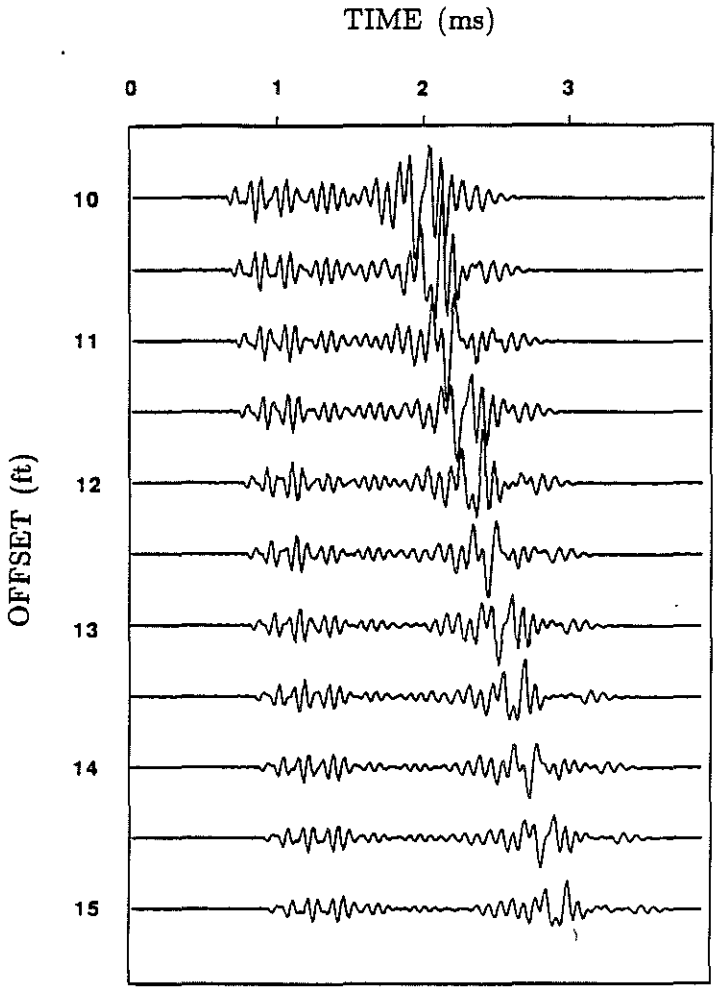

MODEL PARAMETERS

LAYER	OUTER RADIUS (cm)	V_p (km/s)	V_s (km/s)	DENSITY (g/cc)	Q_p	Q_s
fluid	4.699	1.68	0.00	1.20	20.00	0.00
steel	5.715	6.10	3.35	7.50	1000.00	1000.00
cement	6.985	2.82	1.73	1.92	40.00	30.00
fluid	10.160	1.68	0.00	1.20	20.00	0.00
formation	∞	4.00	2.13	2.16	60.00	60.00

sampling interval = 13.333334 μs

Figure 7: Data for a model with unbonded casing.

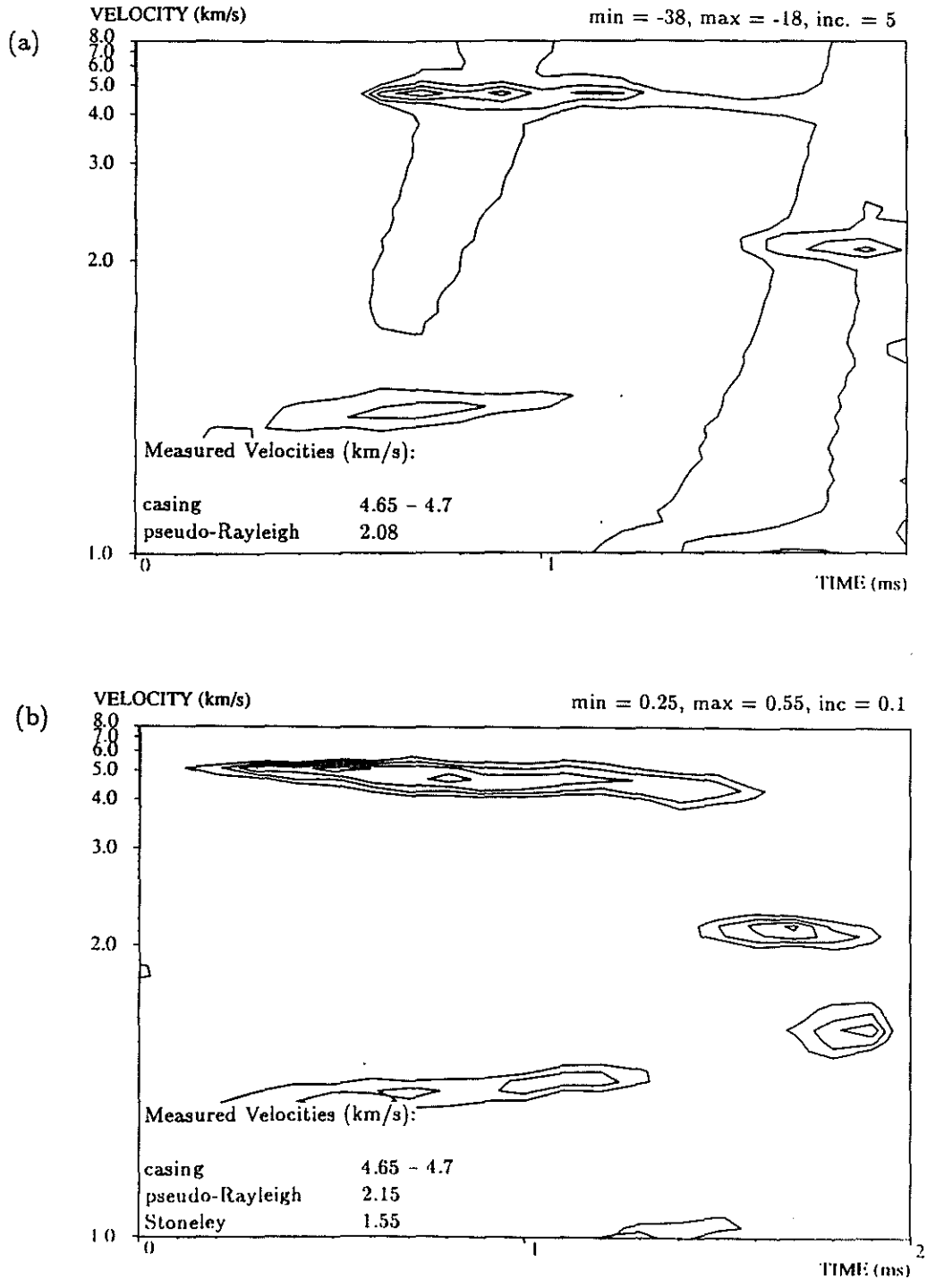

Figure 8: Velocity analysis of the data in Figure 7. (a) Velocity spectrum at 11.7 kHz (b) Semblance

good formation S-wave velocity estimate is obtained. The peaks located at a velocity of about 4.65 to 4.7 km/s on the figures correspond to the casing arrival. There is no peak representing the P wave on either the velocity spectrum or the semblance plot. Apparently these velocity analysis techniques are not powerful enough to separate the P-wave arrival from the complex casing arrival for this model.

Models with lower formation velocities were processed in order to determine when the P-wave arrival can be resolved. A model having a formation P-wave velocity of 3.7 km/s and a S-wave velocity of 1.97 km/s yielded results very similar to those just examined. Results for a model having formation P and S-wave velocities of 3.4 km/s and 1.81 km/s, respectively, are presented in Figures 9a and b. The P wave still cannot be resolved on the velocity spectra, but a weak maximum is present on the semblance plot between 3.4 and 3.45 km/s. The pseudo-Rayleigh wave is represented by a peak at 1.8 km/s on both plots, although on the semblance plot this peak is beginning to merge with the Stoneley-wave maximum. Finally, data from a slow formation are analyzed. The formation P-wave velocity for this model is 2.9 km/s, and the S-wave velocity is 1.52 km/s. A typical velocity spectrum and the semblance plot are shown in Figures 10a and b. A strong peak corresponding to the P wave is seen on the semblance plot, and a smaller maximum occurs on the velocity spectrum. The P-wave velocity measured from these plots is between 2.85 and 2.95 km/s. Hence, an accurate formation P-wave velocity estimate is obtained for this model. Since the formation S-wave velocity is less than the borehole fluid velocity, no shear wave or pseudo-Rayleigh wave is generated.

Unbonded-casing data were also analyzed for the formations with the higher velocities: P-wave velocity = 4.88 km/s (S-wave velocity = 2.6 km/s) and P-wave velocity = 5.94 km/s (S-wave velocity = 3.2 km/s). In each case, the formation S-wave velocity was estimated to within 3% by both methods, but the P wave could not be resolved by either method.

The reason why the P wave is more difficult to resolve in the unbonded-casing situation than in the free-pipe situation is two-fold. First, the casing arrival has a lower velocity in this situation (4.65-4.7 km/s) than in the free-pipe situation (5.3-5.5 km/s). This casing velocity lies near the center of the P-wave velocity range of interest in well logging applications — approximately 3.0 to 6.0 km/s. Thus, the casing arrival affects the resolution of P waves with moderate to relatively low velocities as well as those with high velocities. Secondly, the casing arrival in the unbonded-casing situation is more complex than the steel arrival in the free pipe situation. This complexity seems to hinder the maximum-likelihood method a little more than the semblance method. In the free-pipe situation, separate analysis of different frequency components via MLM offers an advantage because the steel arrival and the P wave attain their maximum power at somewhat different frequencies. In the unbonded-casing situation, this advantage is lost because the addition of the cement layer adds a lower-frequency component to the casing arrival which apparently overlaps much of the main frequency range of the

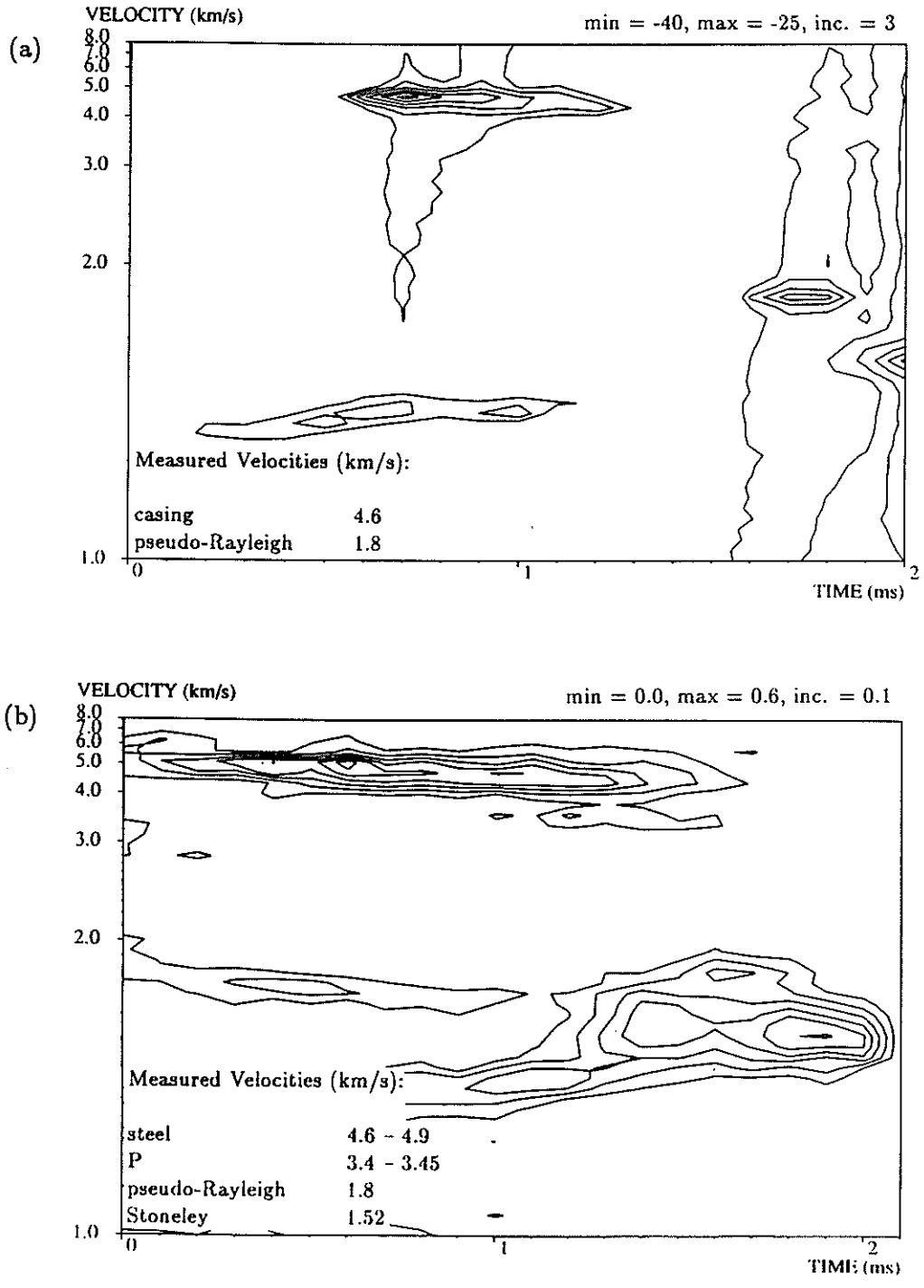

Figure 9: Velocity analysis of unbonded-casing data. The borehole geometry is the same as that shown in Figure 7, but the formation velocities are lower: P-wave velocity = 3.4 km/s, S-wave velocity = 1.81 km/s. (a) Velocity spectrum at 12 kHz (b) Semblance

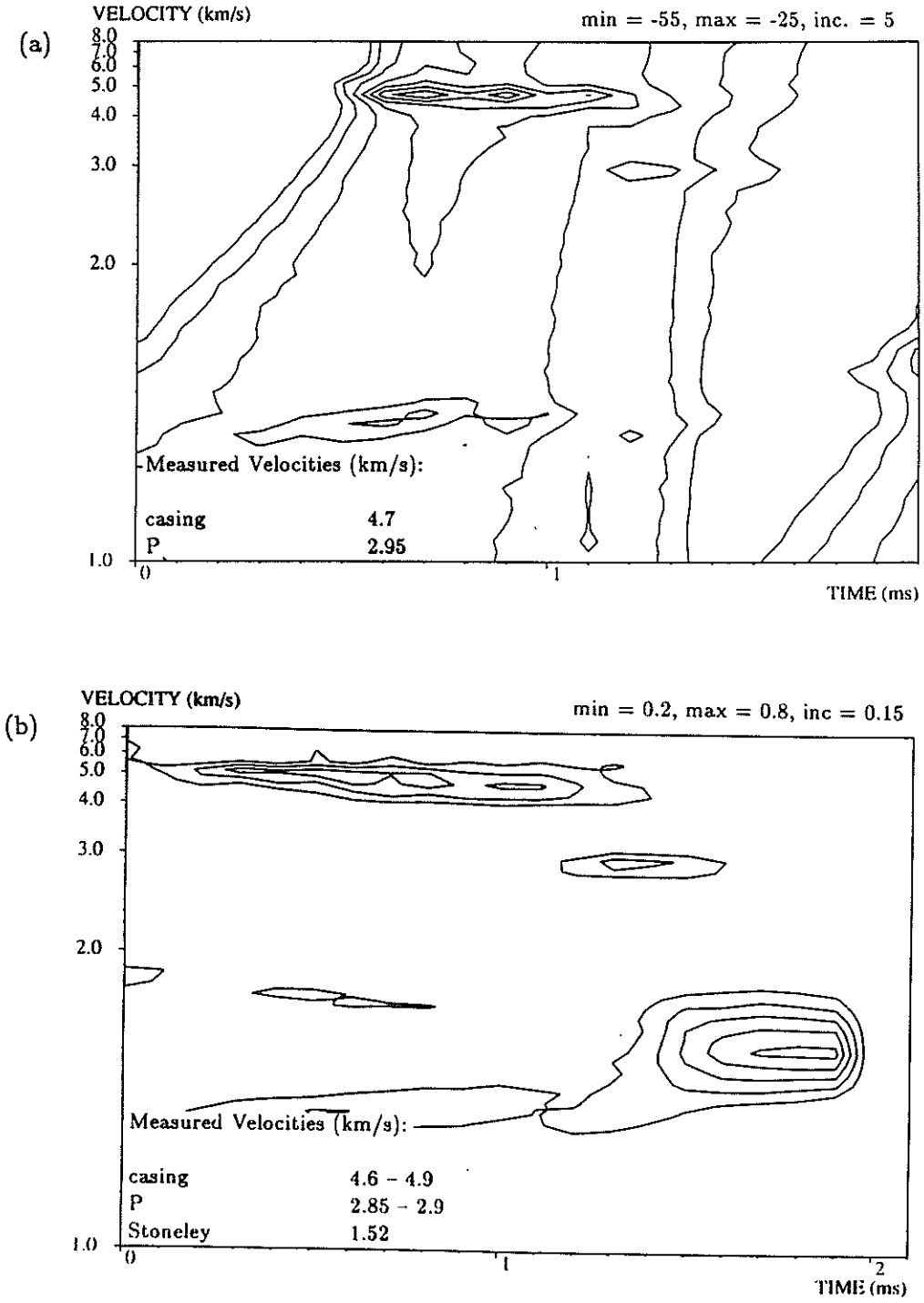

Figure 10: Velocity analysis of data from an unbonded-casing situation in a slow formation. The borehole geometry is the same as that shown in Figure 7, and the formation P and S-wave velocities are 2.9 km/s and 1.52 km/s, respectively. (a) Velocity spectrum at 11.7 kHz (b) Semblance

P wave. When two coherent arrivals with the same frequency and similar slownesses are analyzed by the maximum-likelihood method, the power estimates are biased down. This fact explains why the P wave is not resolved by MLM in most of the models discussed above and why the P-wave maximum is very weak in Figure 10a.

Field Data

Figure 11 contains acoustic logging data from an open borehole. Despite the fact that the data were recorded in an open borehole, there is a rather large amount of ringing in the waveforms. The pseudo-Rayleigh wave clearly has a 'multi-pulse' nature, and the P wave appears to consist of two fairly distinct pulses rather than one. Whether this response is due to one or more reflections or whether it is a result of the nature of the tool, or is possibly due to damage around the borehole cannot be determined from this data set alone. However, other data sets from the same well exhibit the same behavior, lending support to either of the latter two hypotheses. Velocity spectra at 4.7 kHz and 7.8 kHz are presented in Figures 12a and b, respectively, and the semblance is shown in Figure 12c. A P-wave velocity estimate of 6.2 km/s is obtained from Figures 12b and c. (The P wave is not resolved well in Figure 12a because the frequency is low.) The velocity spectrum at 4.7 kHz yields a formation S-wave velocity estimate of about 3.22 – 3.23 km/s, and the semblance plot gives an estimated velocity of about 3.20 km/s. In the velocity spectrum at 7.8 kHz (Fig. 12b), there are two pseudo-Rayleigh wave peaks, one at a velocity of 3.2 km/s and one at a lower velocity of around 2.85 km/s. It is not clear whether these two peaks represent two pseudo-Rayleigh modes, or whether they are simply a result of the complex nature of the waveforms described above.

Figure 13 contains microseismograms from the same well as above, and from the same depth, but after the well was cased. The casing is well-bonded in this part of the well, and thus the first arrival is the P wave. Figure 14a shows the velocity spectrum at 7.8 kHz, and Figure 14b contains the semblance plot. The P wave is represented by a maximum at a phase velocity of 6.3 km/s in the velocity spectrum, and 6.1 km/s in the semblance plot. These results are consistent with those from the open-hole log. In the velocity spectrum at 7.8 kHz, the pseudo-Rayleigh wave is represented by several peaks varying in velocity from about 3.0 to 3.5 km/s. The small peak at a time of 2.85 ms and a velocity of 2.95 km/s is believed to represent the Airy phase of the pseudo-Rayleigh wave. The overall increase in the pseudo-Rayleigh wave velocity is consistent with the theory that the pseudo-Rayleigh wave dispersion curve shifts to higher frequencies when the effective borehole radius decreases due to the casing (Cheng and Toksöz, 1981). Also, this shift of the dispersion curve explains why the pseudo-Rayleigh wave is not resolved in the velocity spectrum at 4.7 kHz for the cased-hole data (not shown). In the semblance plot, the pseudo-Rayleigh wave peak exhibits dispersion, varying in velocity from about 3.15 to 3.4 km/s. The smaller subpeak to the right (centered at

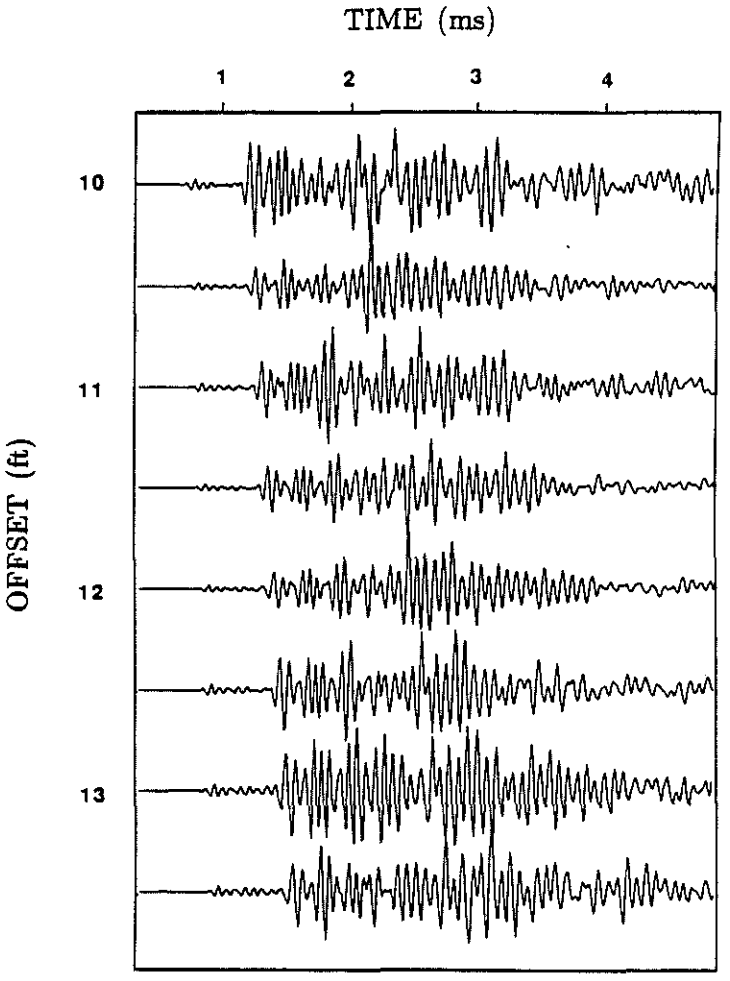

Figure 11: Field data from an open borehole.

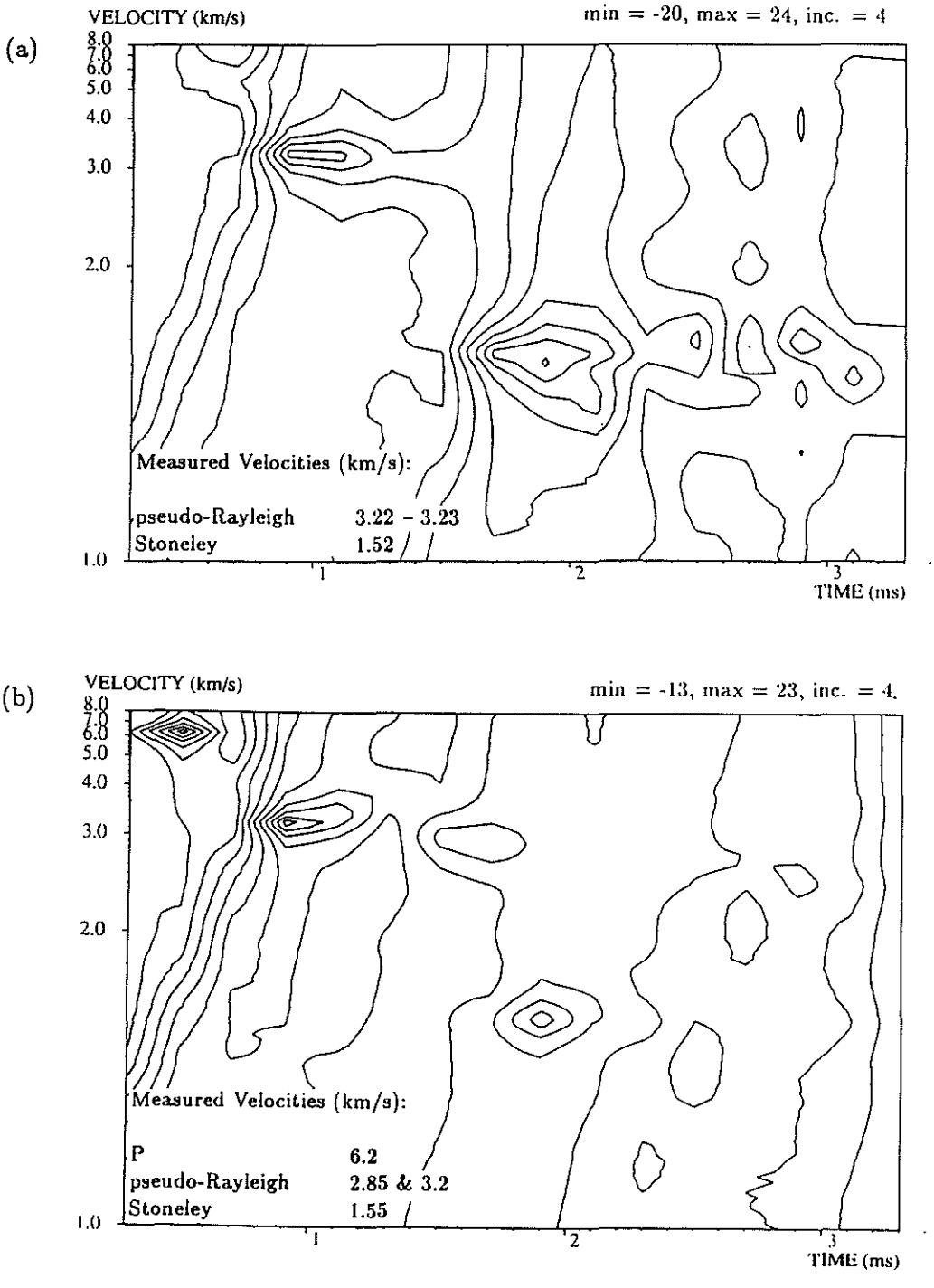

Figure 12: Velocity analysis of the data in Figure 11. (a) Velocity spectrum at 4.7 kHz (b) Velocity spectrum at 7.8 kHz (c) Semblance

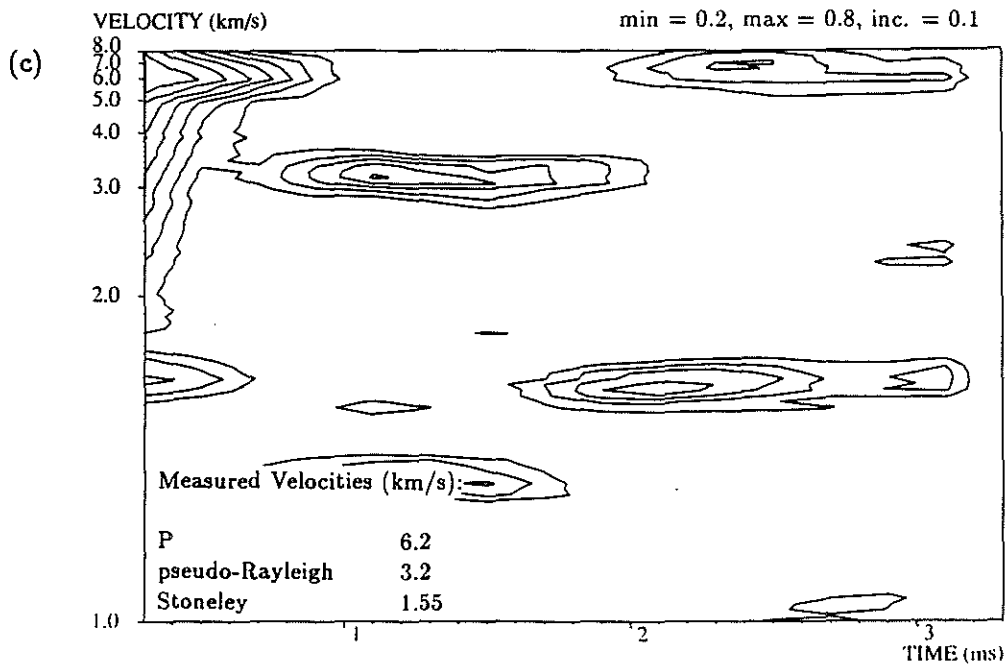

about 2.7 ms) represents the Airy phase and yields a velocity of 3.0 km/s. Recall that no dispersion was noticed in the semblance plot for the open-hole data (Figure 12c). This suggests that the higher frequencies of the pseudo-Rayleigh wave are being excited to a greater degree in the cased hole than in the open hole. This hypothesis could also explain why the Stoneley wave is resolved in the velocity spectrum at 7.8 kHz for the open-hole data but not for the cased-hole data. According to this idea, the pseudo-Rayleigh wave is excited to a greater degree at 7.8 kHz in the cased hole than in the open hole, making the Stoneley wave more difficult to resolve.

The data shown in Figure 15 was recorded in the same well as the previous data but in a different formation. These traces are from the open-hole log. Although the data is noisy, the P wave, the pseudo-Rayleigh wave, and the Stoneley wave can be distinguished. The velocity spectra at 4.7 and 7.8 kHz are presented in Figures 16a and b, and the semblance plot is shown in Figure 16c. The P-wave velocity estimate varies from plot to plot. The velocity spectrum at 4.7 kHz yields an estimate of 5.3 – 5.35 km/s, the spectrum at 7.8 kHz gives a velocity of 5.6 – 5.7 km/s, and from the semblance plot an estimate of about 5.5 km/s is obtained. The values of the formation S-wave velocity estimate range from 2.87 km/s to 3.03 km/s. As in the other data sets, two pseudo-Rayleigh peaks are observed in the velocity spectrum at 7.8 kHz.

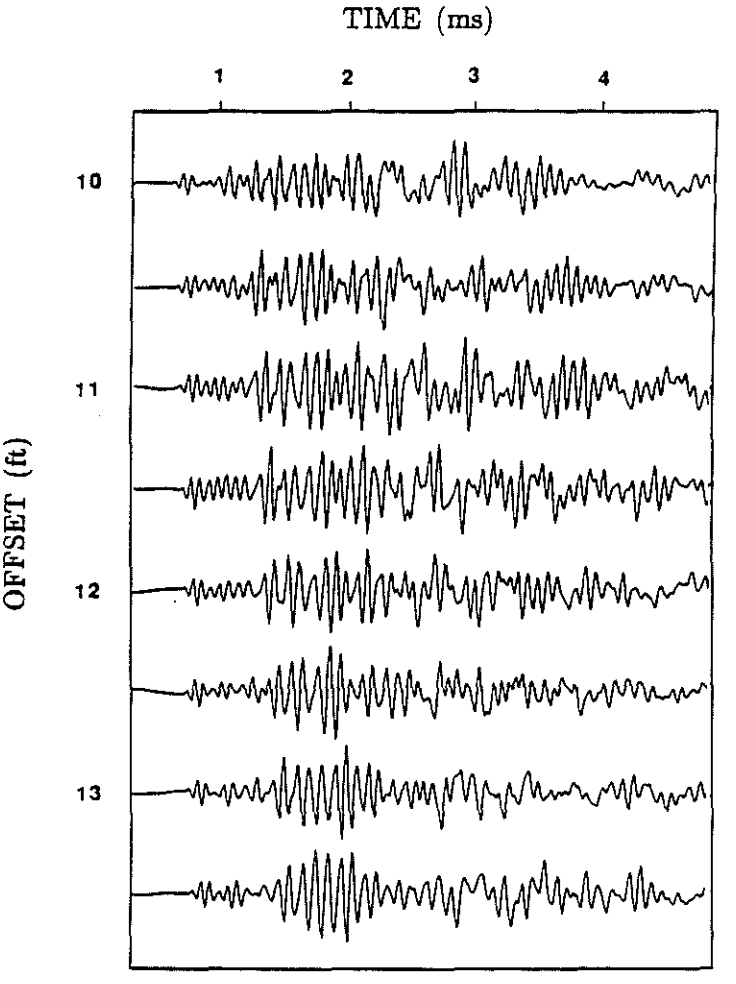

Figure 13: Field data from a well-bonded cased hole. The data is from the same well and the same depth as the data shown in Figure 11.

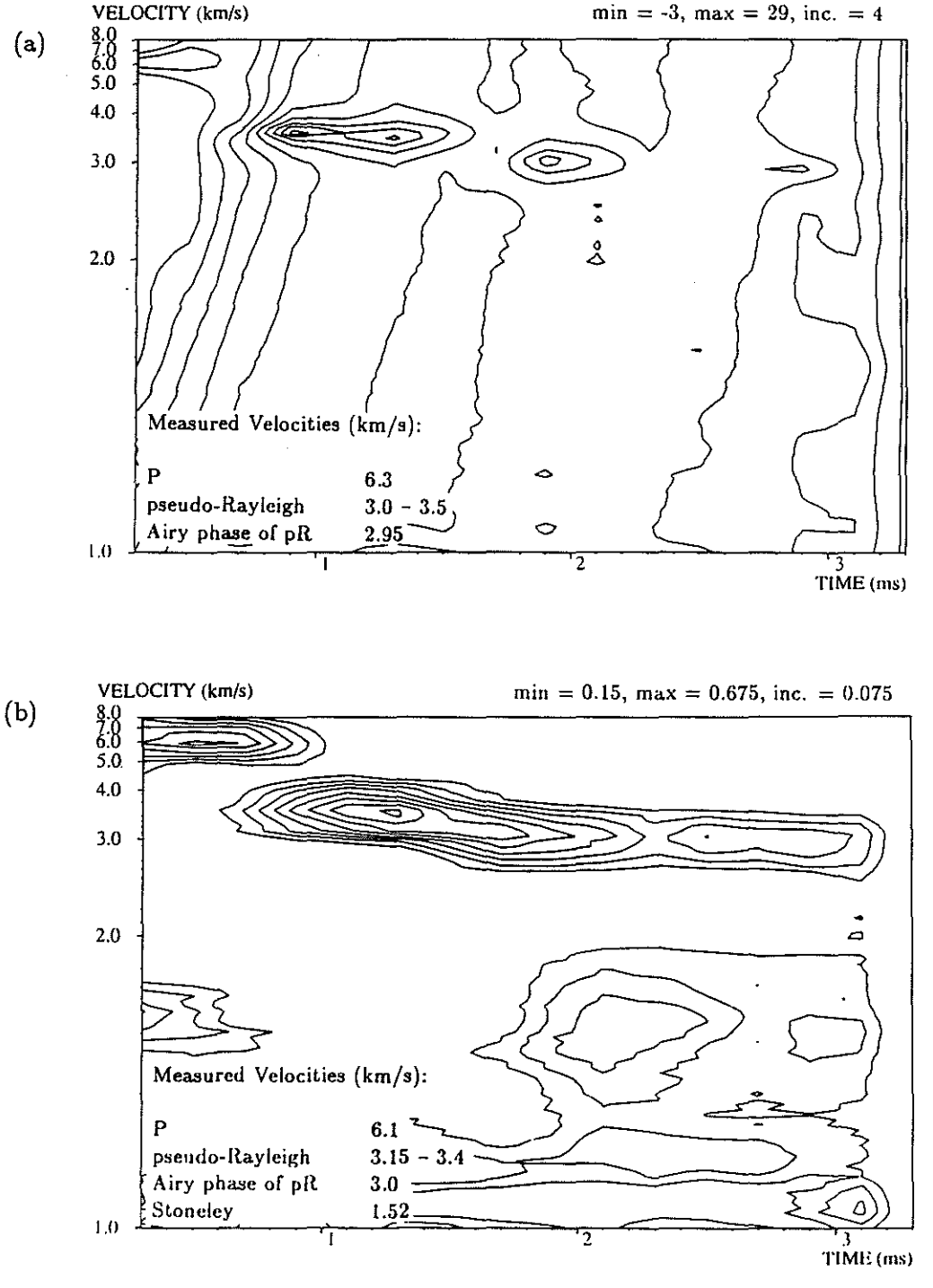

Figure 14: Velocity analysis of the data in Figure 13. (a) Velocity spectrum at 7.8 kHz (b) Semblance

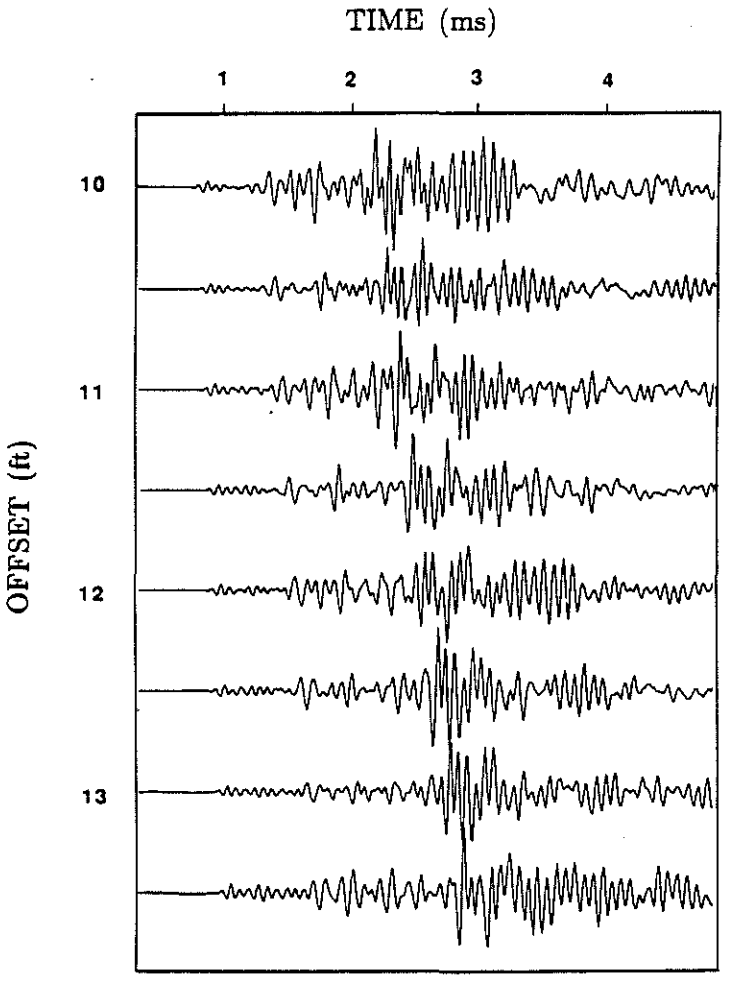

Figure 15: Field data from an open borehole.

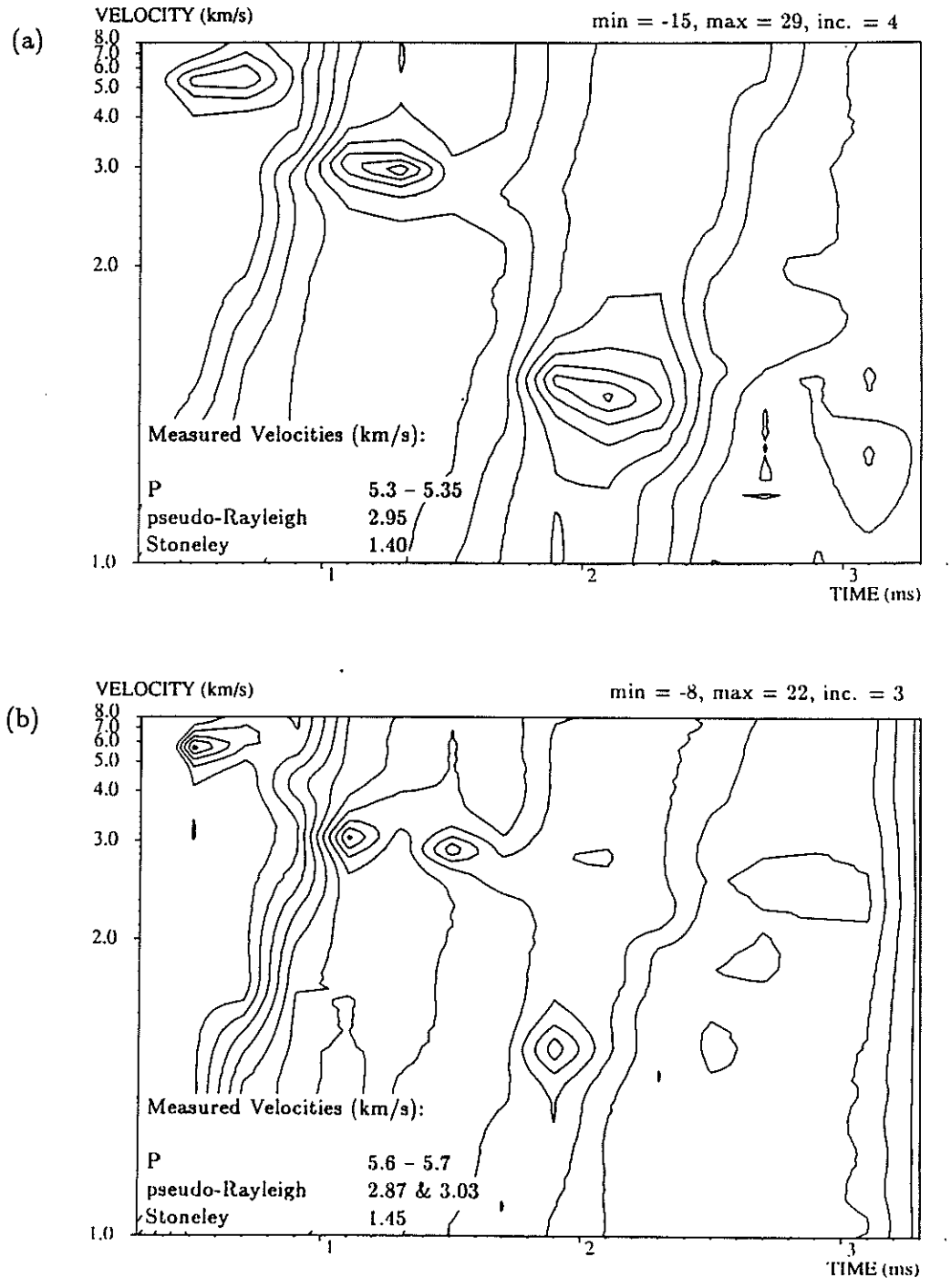

Figure 16: Velocity analysis of the data in Figure 15. (a) Velocity spectrum at 4.7 kHz (b) Velocity spectrum at 7.8 kHz (c) Semblance

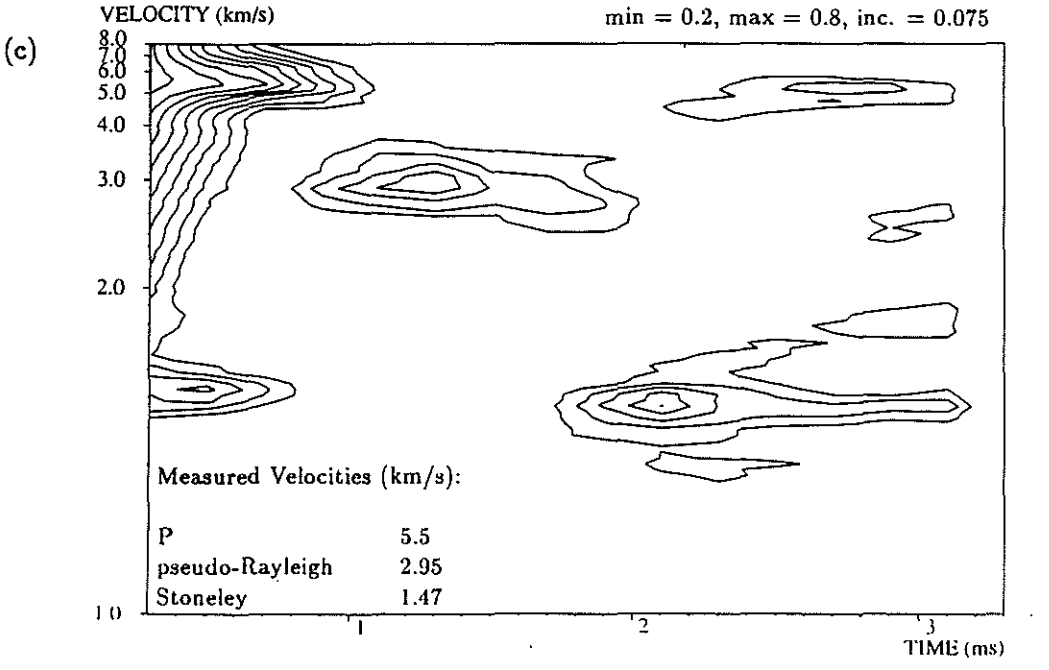

The microseismograms in Figure 17 are from the cased-hole log, at the same depth as the data just examined. The hole was not cemented at this depth — the steel pipe is not bonded to the surrounding rock. Hence, this data corresponds to a special case of the free-pipe situation. Figures 18a and b contain the velocity spectrum at 7.8 kHz and the semblance contour plot, respectively. Five arrivals are resolved on the velocity spectrum: the Stoneley wave at a velocity of about 1.53 km/s, the shear/pseudo-Rayleigh arrival at a velocity of 2.9 to 2.95 km/s, the Airy phase of the pseudo-Rayleigh wave at a velocity of 2.6 km/s, and two arrivals at relatively high velocities of approximately 5.0 km/s and 5.5 – 5.6 km/s. From analysis of the open hole data, the P wave is expected to have a velocity between 5.3 and 5.7 km/s. The steel arrival, however, also travels with a velocity in this range, and hence it is impossible to determine which maximum corresponds to the P wave and which one corresponds to the steel arrival. In practice, continuity of the peaks over a range of depths would be needed to correctly identify the two arrivals. On the semblance plot (Figure 18b) there is only one high-velocity arrival (at 5.5 km/s). This lack of resolution in the semblance results is consistent with earlier analysis of synthetic data (Recall Figure 4d). Maxima representing the shear/pseudo-Rayleigh wave and the Stoneley wave are present in the semblance results. However, these maxima are not prominent due to the large amount of interference from the steel arrival. The S-wave velocity estimated from this plot is 2.7 km/s. This data set was low-pass filtered several times to attempt to improve the semblance results. The

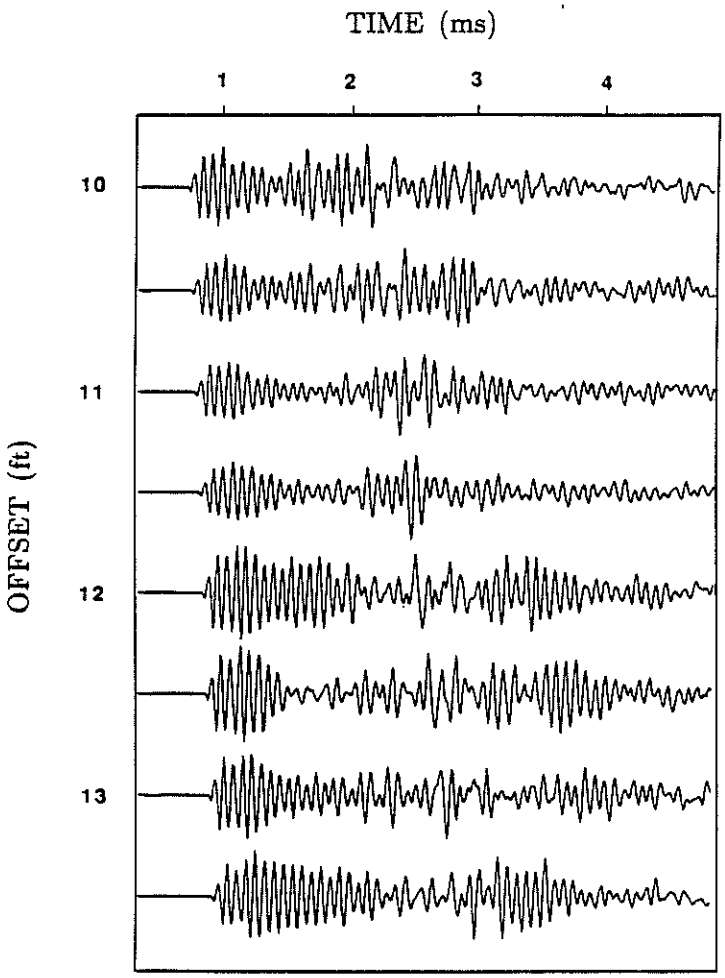

Figure 17: Field data recorded in a borehole with a 'free pipe'. This data is from the same well and the same depth as the data shown in Figure 15.

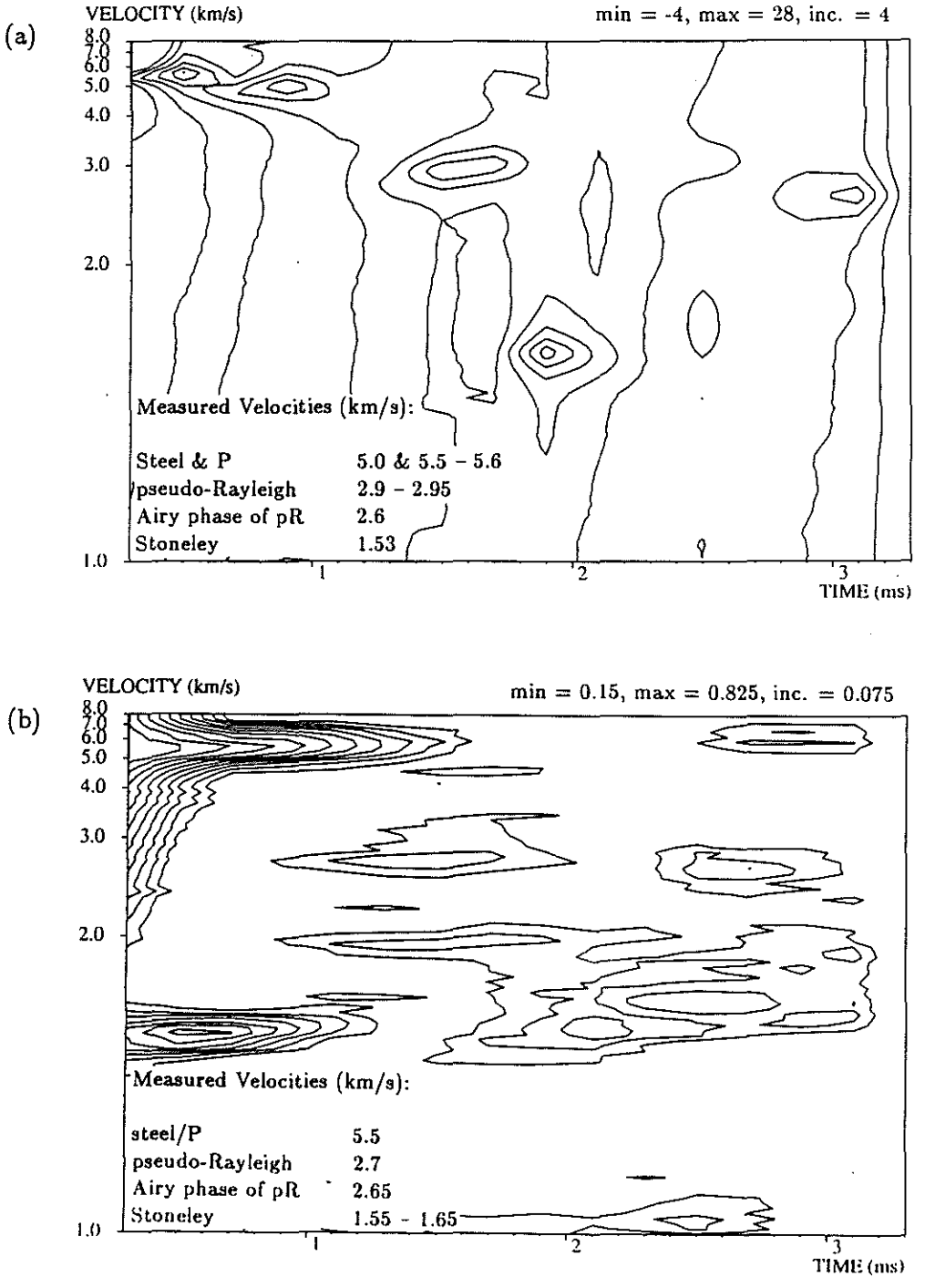

Figure 18: Velocity analysis of the data in Figure 17. (a) Velocity spectrum at 7.8 kHz (b) Semblance

filtering greatly enhanced the overall quality of the semblance plots, but two distinct high-velocity events (i.e., the P wave and the steel arrival) could not be resolved in any of the results. One of the filters used is shown in Figure 19a, and the corresponding filtered traces are presented in Figure 19b. The results of applying the semblance method to this filtered data are shown in Fig. 19c.

CONCLUSIONS

The average semblance and the maximum-likelihood spectral analysis yield good results for synthetic open-hole data. The estimated formation velocities vary by not more than 4% from the true velocities. For synthetic data from well-bonded cased boreholes, the results are generally about the same as for open holes. However, for very fast formations (having a P-wave velocity close to that of the steel pipe), there may be a resonance effect that appears to slow down the P wave slightly.

The major conclusions from analysis of data from poorly-bonded cased-hole models are summarized in Table 2. For cased-hole models with no steel/cement bonding (the free-pipe situation), the measured formation P-wave velocities are approximately 6 to 8% less than the actual velocities. Thus, the greater the formation P-wave velocity, the poorer the velocity estimate. Also, if the formation S-wave velocity is relatively high (about 2.5 km/s or greater), then the S-wave velocity estimate may also be on the order of 8% low. This decrease in the measured velocities is apparently due to the influence of the cement and fluid layers on the propagation of the P and shear/pseudo-Rayleigh waves. The velocity estimates become even worse when the thickness of the fluid layer or the cement layer is increased. Thus, variations in the thickness of the cement layer and/or the fluid layer in the free pipe situation may produce perturbations in the velocity log which are not related to any change in the character of the formation. Furthermore, when the formation P-wave velocity is relatively close to the steel velocity (within roughly 15%), the P-wave arrival cannot be separated from the steel arrival by applying the semblance method to the raw data. The two arrivals are resolved by spectral analysis, although the quality of resolution may vary with frequency. Initial tests show that the P wave may be resolved by the semblance method for this situation if the data is first low-pass filtered. However, the resulting velocity estimate is affected by the filtering process. Further details of this approach have not been pursued in this study.

For cased-hole models with no cement/formation bonding (the unbonded-casing situation), neither velocity analysis method can resolve the P-wave arrival when the P-wave velocity differs from the velocity of the casing arrival by less than about 28%. The semblance method gives better results than MLM in marginal cases. For example, for the casing parameters used in these studies, the casing arrival has a velocity of 4.65

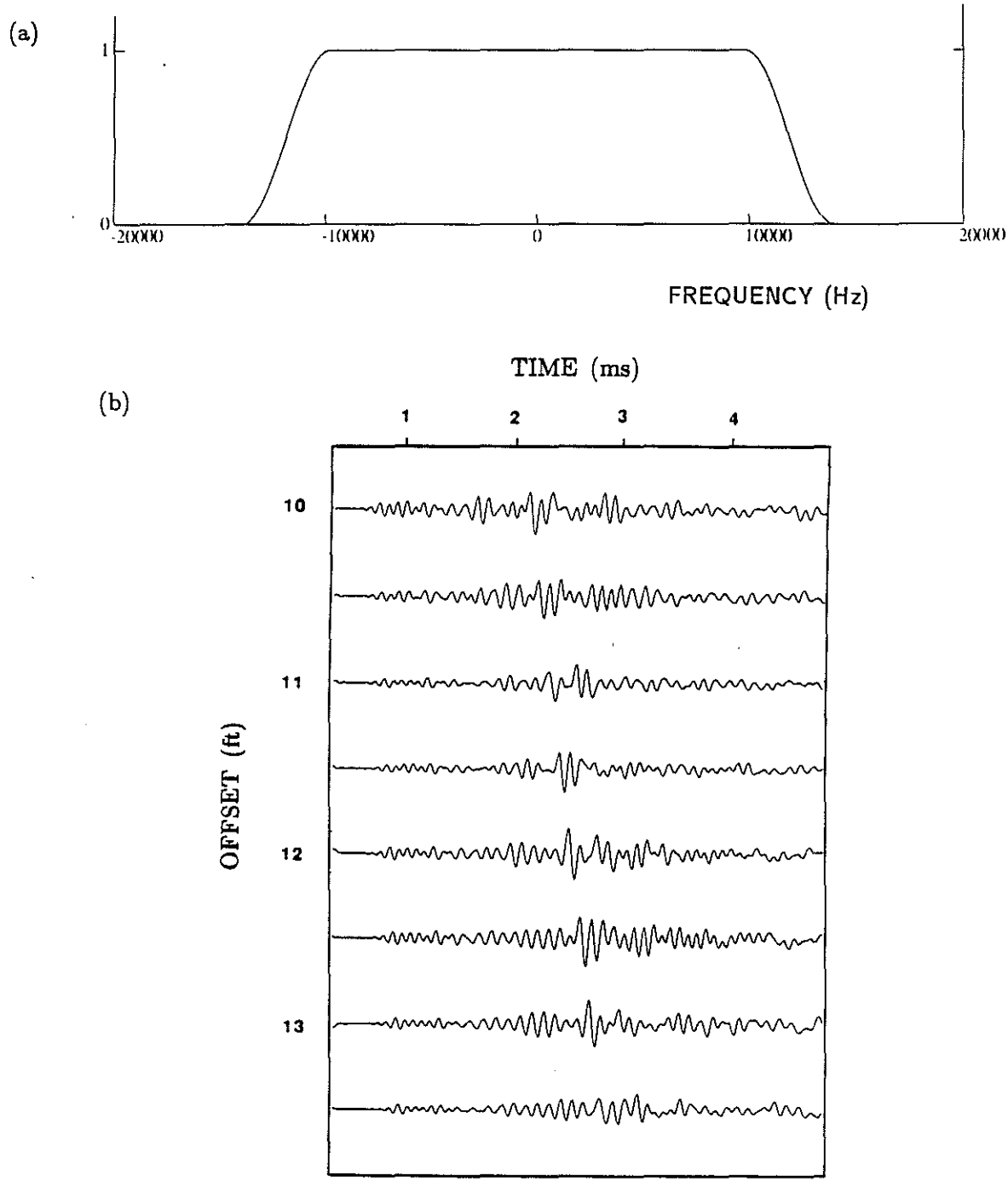

Figure 19: (a) Low-pass filter applied to the data in Figure 17. (b) Filtered data. (c) Semblance results from the filtered data.

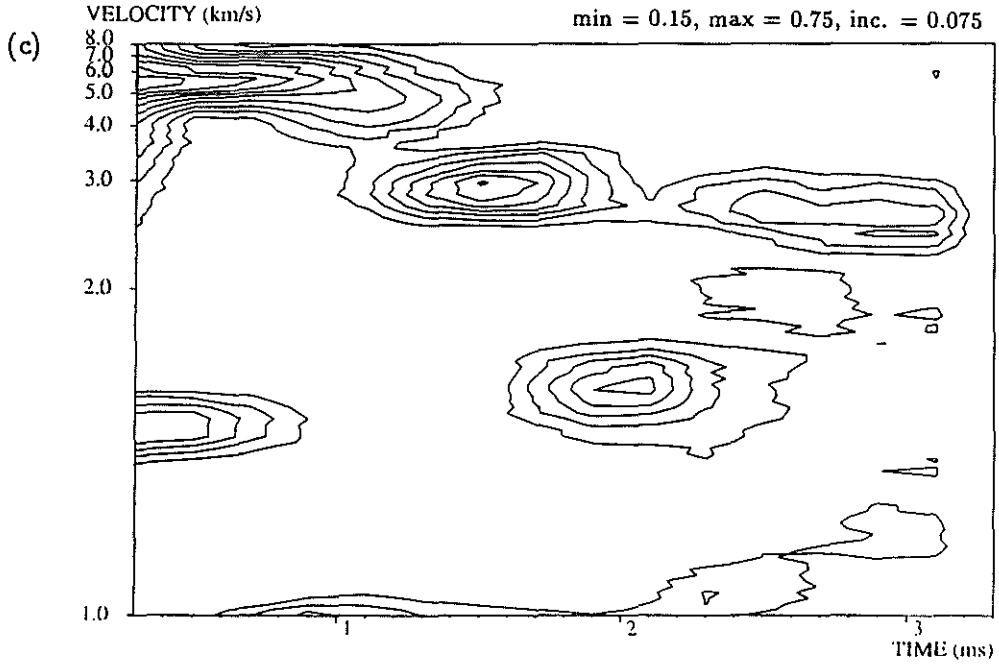

km/s. For models with P-wave velocities ranging from 3.4 km/s to 5.94 km/s, the P wave cannot be resolved by the maximum-likelihood method. This arrival is resolved by the semblance method only for the model with the P-wave velocity of 3.4 km/s. (The correct velocity of 3.4 km/s is obtained.) For all of these models, the formation S-wave velocity is determined by both methods to within 3% relative error. Also, for a slow formation (P-wave velocity = 2.9 km/s), the formation P-wave velocity is estimated to within 2% error by both methods. The inability of either method to resolve the P wave over a large range of velocities greatly reduces the usefulness of data recorded in holes with unbonded casing.

Although not presented in this report, models having fewer receivers (as few as four) and a larger receiver spacing (1.0 ft.) were analyzed. When the number of receivers is decreased, the peaks corresponding to the casing, P, pseudo-Rayleigh, and Stoneley arrivals are still present. However, the velocity resolution is decreased, and the aliasing peaks on the MLM plots are increased in amplitude. In some cases the aliasing peaks are about as strong as the main peaks. When the receiver spacing is increased from 0.5 ft. to 1.0 ft., the main peaks can still be identified, but the number of aliasing peaks on the MLM plots and the number of cycle-skipping peaks on the semblance plot increase.

The field data which has been analyzed thus far supports the results found from

Formation Velocities	Free-pipe		Unbonded-Casing	
	MLM	Semblance	MLM	Semblance
Very Slow (no S-wave)	OK *	OK *	OK	OK
Slow	OK *	OK *	cannot separate P wave from casing arrival	weak but distinguishable P-wave maximum
Moderate	OK	OK	cannot separate P-wave from casing arrival	cannot separate P wave from casing arrival
Fast	OK	filtering required to separate P-wave from casing arrival	cannot separate P wave from casing arrival	cannot separate P wave from casing arrival
Very Fast (P-wave vel. $\approx$ 6 km/s)	cannot separate P wave from casing arrival	cannot separate P wave from casing arrival	cannot separate P wave from casing arrival	cannot separate P wave from casing arrival

Table 2: Summary of the major conclusions from analysis of synthetic acoustic logging data for free-pipe and unbonded-casing situations. The * denotes situations that were not modelled - these conclusions were deduced from the other results.

the study of the synthetic data. The maximum-likelihood method and the semblance method generally work well in data from open holes and well-bonded cased holes. The maximum-likelihood method has been found to yield better results than the semblance method on data recorded in a free pipe in a formation having a P-wave velocity of about 5.5 km/s. In other free pipe situations, in formations having lower velocities, both methods have been found to work equally well. No data recorded in a well with unbonded casing has yet been analyzed.

ACKNOWLEDGEMENTS

This work was supported by the Full Waveform Acoustic Logging Consortium at M.I.T. Lisa Block was also supported by the Phillips Petroleum Fellowship.

REFERENCES

Cheng, C. H., and Toksöz, M. N., 1981, Elastic wave propagation in a fluid-filled borehole and synthetic acoustic logs; Geophysics, 46, 1042–1053.

Duckworth, G. L., 1983, Processing and inversion of Arctic Ocean refraction data; Sc.D. thesis, Joint Program in Ocean Engineering, Mass. Inst. Tech., Cambridge, Massachusetts, and Woods Hole Oceanographic Institution, Woods Hole, Massachusetts.

Tubman, K. M., 1984, Full waveform acoustic logs in radially layered boreholes: Ph.D. thesis, Mass. Inst. Tech., Cambridge, Massachusetts.

Tubman, K. M., Cheng, C. H., and Toksöz, M. N., 1984, Synthetic full waveform acoustic logs in cased boreholes; Geophysics, 49, 1051–1059.

APPENDIX – VELOCITY ANALYSIS

Windowing the Data

The velocity analyses are implemented within short time windows of given moveout across the receiver array. An example of such a window is shown in Figure A - 20. τ is the beginning time of the window on the near trace, T is the length of the window, and v is the slope (dx/dt) of the window. v is equal to a trial phase velocity in the direction of the array. For receivers in a borehole, the signals travel essentially parallel to the array, and hence v is equal to the phase velocity of propagation. (The paths taken from the tool to the borehole wall and vice versa require about the same amount of time for each receiver and hence do not significantly affect the moveout of the signal.) For a fixed time τ, calculations are made for many different slownesses. The window is then advanced by a small amount, dr, and the process is repeated. The final result is a series of contour plots. Each plot is a function of time τ and velocity v. One plot is obtained from the semblance method and several plots are obtained from the maximum-likelihood method, each at a fixed frequency. As will be seen below, the output of the maximum-likelihood

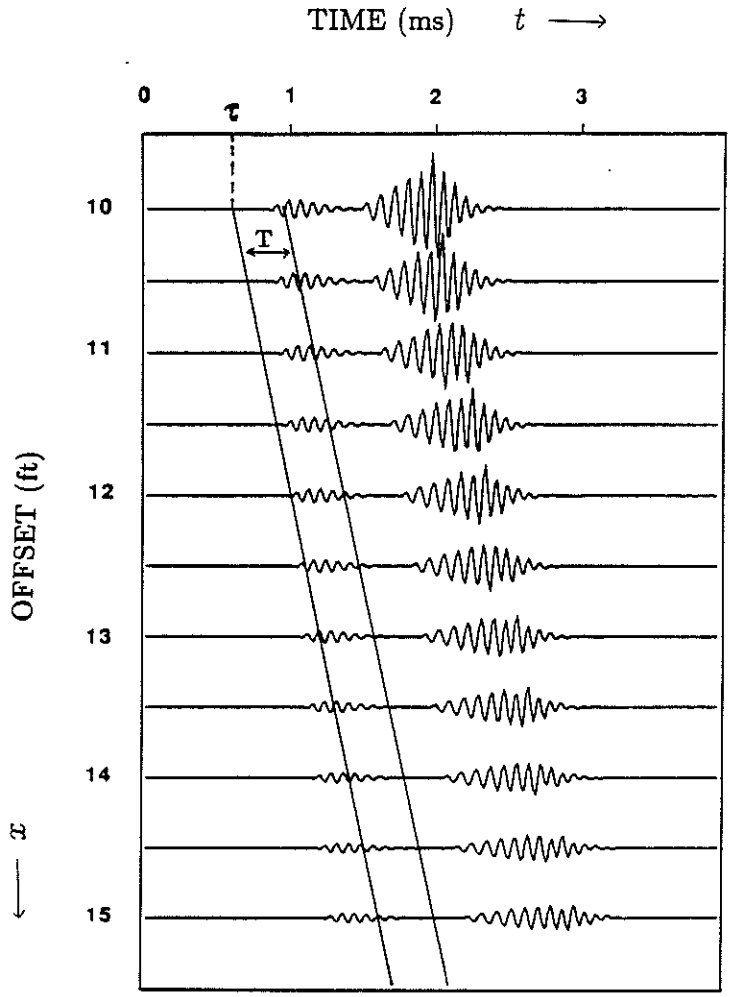

Figure A - 20: Window Parameters

method is proportional to slowness p, rather than velocity. To maintain equal resolution across the contour plots, the calculations are made at equal increments of p, and so the velocity axis is linear in slowness.

Average Semblance

The average semblance is the ratio of the energy of a stacked trace to the sum of the energies of the individual traces within a time window, divided by the number of traces. Let $x(t, z_k)$ represent the time series at distance z_k. Then the average semblance within the time window at position τ with moveout v (Recall Figure A - 20) is given by:

$$Semblance_{avg}\left(\tau, v = \frac{1}{p}\right) = \frac{\sum_{t_k=\tau+pz_k}^{\tau+pz_k+T}\left(\sum_{k=0}^{N-1} x(t_k, z_k)\right)^2}{N\sum_{t_k=\tau+pz_k}^{\tau+pz_k+T}\sum_{k=0}^{N-1}\left(x(t_k, z_k)\right)^2}.$$

The values of average semblance range from zero to one.

The Maximum-Likelihood Method

This method essentially consists of computing a two-dimensional Fourier transform within the time window. The output is power, contoured in dB. Let $x(t, z_k)$ represent the time series at distance z_k, as defined previously. For simplicity, the near trace in the data set is taken to be at distance 0, i.e., $z_0 = 0$. An estimate of the temporal Fourier transform of the data within the time window illustrated in Figure A - 20, for the receiver located at distance z_k, is given by:

$$X(\tau, \omega, z_k) = e^{-i\omega z_k p}\int_{\tau}^{\tau+T} x(t + z_k p, z_k)\ w(t - \tau)\ e^{i\omega t}\ dt.$$

Recall that τ is the beginning time of the window on the near trace, T is the length of the window in time, and p is the slowness associated with the moveout of the window across the traces. Since a shift in the time domain corresponds to multiplication by a complex exponential in the frequency domain, the term in front of the integral must be included to restore the proper phase to the spectrum. $w(t)$ is a window function which is used to improve the resolution of the estimated spectrum. The estimated spectrum is the true frequency spectrum of the data within the short time window convolved with the frequency spectrum of the window function. (This distortion is the 'smearing' of the frequency spectra which is referred to in the text.) The window function used in this study is $sin^2\left(\frac{t\pi}{T}\right)$. In practice, this integral must be converted into a summation

(i.e., a discrete Fourier transform or DFT). The Fourier coefficients for all frequencies (up to the Nyquist frequency) are computed simultaneously using an FFT algorithm.

At a fixed frequency, ω_o, an estimate of the spacial transform may be obtained by summing across the receivers as follows:

$$X(\tau, \omega_o, p) = \sum_{k=0}^{N-1} a_k \; X(\tau, \omega_o, z_k) \; e^{-i\omega_o p z_k} \; \delta z$$

where N is the number of receivers in the array and δz is the receiver spacing. Since wavenumber k is equal to $\omega_o p$, with ω_o fixed, the transform has been written as a function of slowness p rather than wavenumber. The a_k are 'weights' on the receivers which perform the same function in the spacial transform that the window function $w(t)$ performs in the temporal transform. The estimated spacial transform, $X(\tau, \omega_o, p)$, is the actual transform of the data convolved with the spacial transform of the weight function $(a_0, a_1, ..., a_{N-1})$. In conventional spectral analysis, also called beamforming, these weights are fixed while the Fourier coefficients are computed for all wavenumbers, or slownesses, of interest. In the maximum-likelihood method, however, a new set of weights is determined for each slowness considered. This procedure improves the resolution of the final velocity spectrum, since it decreases interference from components traveling with nearby slownesses. The way in which the a_k are determined will be addressed shortly. The previous equation may be rewritten in vector form as:

$$X(\tau, \omega_o, p) = \underline{A}^* \; \underline{X}$$

where

$$\underline{A} = \begin{bmatrix} a_0 e^{i\omega_o p z_0} \; \delta z \\ a_1 e^{i\omega_o p z_1} \; \delta z \\ \cdot \\ \cdot \\ \cdot \\ a_{N-1} e^{i\omega_o p z_{N-1}} \; \delta z \end{bmatrix}, \quad \underline{X} = \begin{bmatrix} X(\tau, \omega_o, z_0) \\ X(\tau, \omega_o, z_1) \\ \cdot \\ \cdot \\ \cdot \\ X(\tau, \omega_o, z_{N-1}) \end{bmatrix}$$

and * denotes complex conjugate transpose. The estimate of the power due to the plane wave component traveling with slowness p at frequency ω_o is:

$$P_x(\tau, \omega_o, p) = \frac{\| \; X(\tau, \omega_o, p) \; \|^2}{T} = \frac{\| \; \underline{A}^* \; \underline{X} \; \|^2}{T} = \underline{A}^* \; \underline{\mathbf{K}_x} \; \underline{A}$$

where $\underline{\mathbf{K}_x} \left(= \frac{\underline{X} \; \underline{X}^*}{T} \right)$ is an estimated spectral covariance matrix.

In order to determine the optimum weights (a_k), two issues must be considered. First, when a certain slowness p is being scanned, it is required that the contribution to the power estimate due to a plane wave component propagating with that slowness be unbiased. To state this mathematically, let $Be^{i\omega_o p z_k}$ represent the temporal Fourier

transform (at frequency ω_o) of the plane wave component of interest at receiver k. Then we require that:

$$\frac{\| \underline{A}^* \, B\underline{E} \|^2}{T} = \frac{B^2}{T}$$

where

$$\underline{E} = \begin{bmatrix} e^{i\omega_o p z_0} \\ e^{i\omega_o p z_1} \\ \cdot \\ \cdot \\ \cdot \\ e^{i\omega_o p z_{N-1}} \end{bmatrix}.$$

This reduces to:

$$\underline{A}^* \, \underline{E} = 1.$$

Another way to think about this constraint is that we are requiring the spacial transform of the weight function $(a_0, a_1, ..., a_{N-1})$ to have a value of 1 at $p = 0$. Thus, when this transform is convolved with the spacial transform of the plane wave component at p, a value of B will be obtained as required. Although the contribution to the power estimate from the plane wave component with slowness p is unbiased, the total power estimate may still be wrong due to 'contamination' from components with nearby slownesses. To reduce this problem, the total power estimate is minimized:

$$min \left(\underline{A}^* \, \underline{\mathbf{K}_x} \, \underline{A} \right).$$

Hence, we wish to minimize the total power estimate, $\underline{A}^* \, \underline{\mathbf{K}_x} \, \underline{A}$, subject to the constraint $\underline{A}^* \, \underline{E} = 1$. Using the Lagrange multiplier method, it can be shown that the matrix $\underline{A}$ which satisfies these requirements is given by:

$$\underline{A} = \frac{\underline{\mathbf{K}_x}^{-1} \, \underline{\mathbf{E}}}{\underline{\mathbf{E}}^* \, \underline{\mathbf{K}_x}^{-1} \, \underline{\mathbf{E}}}.$$

Substituting this result into the expression for the power estimate yields:

$$P_x(\tau, \omega_o, p) = \frac{1}{\underline{E}^* \, \underline{\mathbf{K}_x}^{-1} \, \underline{\mathbf{E}}}.$$

To summarize the procedure, for a fixed window position, (τ, p), an FFT is performed on each trace to yield all of the frequency coefficients at one time. A spectral covariance matrix is then formed for each frequency of interest. The power estimate is computed via the above formula for each frequency. This procedure is repeated for each new window position. The final result is a series of contour plots. Each plot is a function of τ and p at a fixed frequency.